Abundant Seamounts of the Rano Rahi Seamount Field Near the Southern East Pacific Rise, 15° S to 19° S

DANIEL S. SCHEIRER[1], now at [2], KEN C. MACDONALD[1], DONALD W. FORSYTH[2], YANG SHEN[2], now at [3]

[1]*Department of Geological Sciences, UCSB, Santa Barbara, CA 93106.*
[2]*Department of Geological Sciences, Box 1846, Brown University, Providence, RI 02912.*
[3]*Department of Geology and Geophysics, WHOI, Woods Hole, MA 02543.*

(Received 9 December 1994; revised version 20 July 1995)

Key words: East Pacific rise, seamounts, seafloor volcanism, MELT

Abstract. A widespread seamount province, the Rano Rahi Field, is located near the superfast spreading Southern East Pacific Rise (SEPR) between 15°–19° S. Particularly abundant volcanic edifices are found on Pacific Plate aged 0 to ~ 6.5 Ma between 17°–19° S, an area greater than 100,000 km^2. The numbers of seamounts and their volume are several times greater than those of a comparably-surveyed area near the Northern East Pacific Rise (NEPR), 8°–17° N. Most of the Rano Rahi seamounts belong to chains, which vary in length from ~ 25 km to > 240 km and which are very nearly collinear with the Pacific absolute and relative plate motion directions. Bends of 10°–15° occur along a few of the chains, and some adjacent chains converge or diverge slightly. Many seamount chains have fluctuations in volume along their length, and statistical tests suggest that some adjacent chains trade-off in volume. Several seamount chains split into two lines of volcanoes approaching the axis. In general, seamount chains composed of individual circular volcanoes are found near the axis; the chains consist of variably-overlapping edifices in the central part of the survey; to the west, volcanic ridges predominate. Near the SEPR, the volume of near-axis seamount edifices is generally reduced near areas of deflated cross-sectional area of the axial ridge. Fresh lava flows, as imaged by sidescan sonar and sampled by dredging, exist around some seamounts throughout the entire survey area, in sharp contrast to the absence of fresh flows beyond ~30 km from the NEPR. Also, the increases in seamount abundance and volume extend to much greater crustal ages than near the NEPR. Seamount magnetization analysis is also consistent with this wider zone of seamount growth, and it demonstrates the asynchronous formation of most of the seamount chains and volcanic ridges. The variety of observations of the SEPR seamounts suggests that a number of factors and mechanisms might bring about their formation, including the mantle upwelling associated with superfast spreading, off-axis mantle heterogeneities, miniplumes and local upwelling, and the vulnerability of the lithosphere to penetration by volumes of magma. In particular, we note the association of extensive, recent volcanism with intermediate wavelength gravity lineament lows on crust aged ~ 6 Ma. This suggests that the lineaments and some of the seamounts share a common cause which may be related to ridge-perpendicular asthenospheric convection and/or some manner of extension in the lithosphere.

Marine Geophysical Researches **18:** 13–52, 1996.

Introduction

Oceanic volcanoes provide insight into both the modes of melt generation in the mantle and the nature of its ascent through the lithosphere. These, in turn, are related to mantle upwelling, mantle heterogeneity, and properties of the plate. We include in our definition of near-axis seamounts those volcanoes which form in the vicinity of mid-ocean ridges, but not within the neovolcanic zone itself (such as those in the median valley of the Mid-Atlantic Ridge (Smith and Cann, 1992)). Near-axis seamounts are distinguishable from hotspot seamounts and islands by their much smaller size, much greater abundance, and geochemical affinity to mid-ocean ridge basalt (MORB). Hotspot volcanoes may form on lithosphere of great age. Following other recent studies based on modern echosounder data, we apply the term seamount to features much smaller than the 500 fathom or 1 km minimum height limit defined by Menard (1964).

On recent surveys of the Southern East Pacific Rise (SEPR) and its flanks from 15°–19° S, Figure 1, we discovered an extensive field of abundant seamounts, the Rano Rahi Field ("Many Volcanoes" in the language of Easter Island) (Scheirer *et al.*, 1993; Shen *et al.*, 1993). In a companion paper, Scheirer *et al.* (this issue), we present a series of large-scale maps which illustrate many of the volcanic edifices. The greatest abundance of seamounts occurs on the Pacific Plate between 17° and 19° S, from the EPR axis to ~ 118° W (crustal ages 0.0 to ~ 6.5 Ma). Beyond simply their great abundance, these seamounts exhibit a number of striking features including: new seamount formation and edifice growth scattered throughout the area, arrangement in long chains virtually parallel to the plate motion vectors of the Pacific Plate, and a change in seamount chain morphology from individual edifices to overlapped volcanoes to linear volcanic ridges with

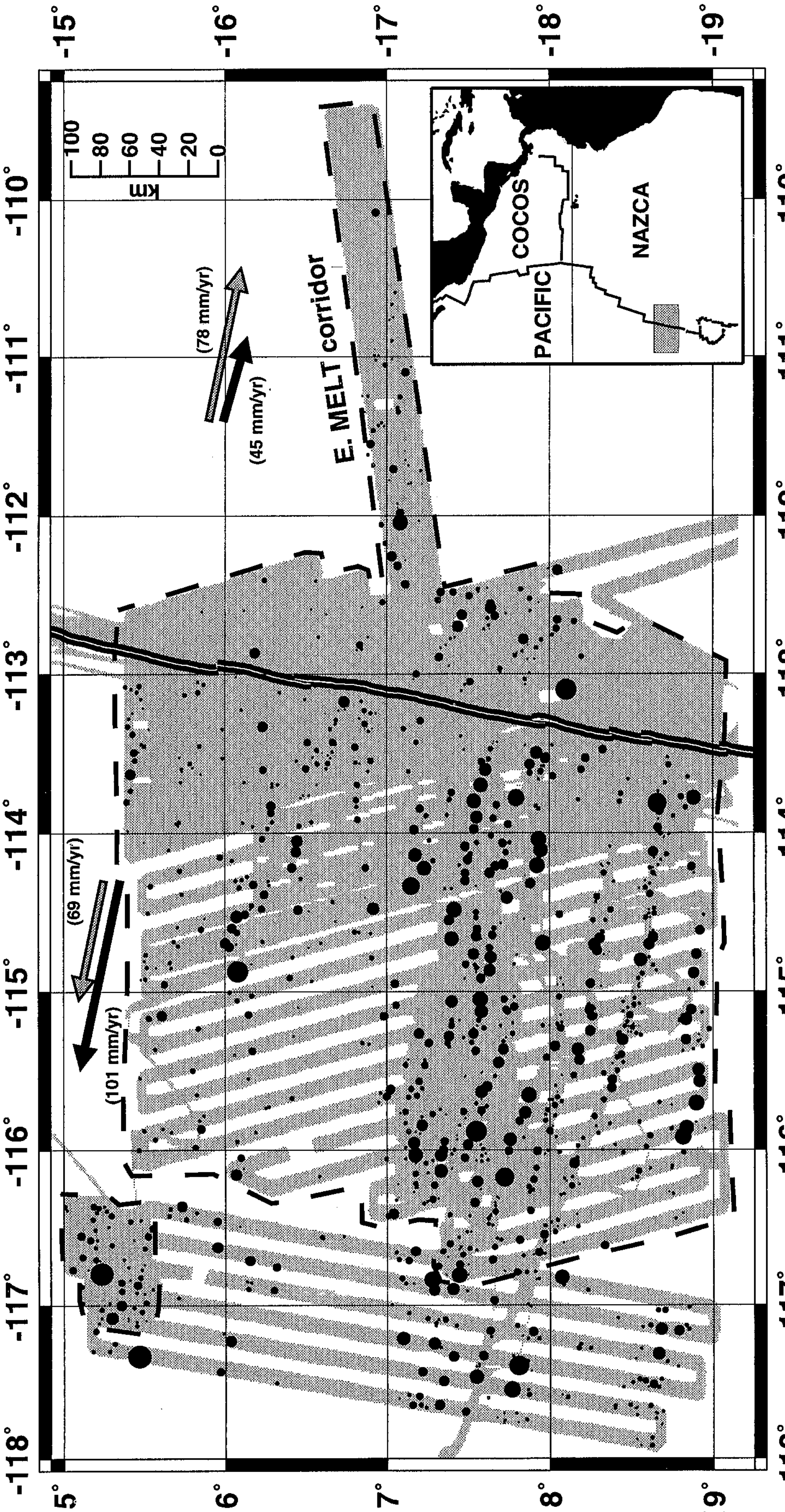

E. MELT corridor
(78 mm/yr)
(45 mm/yr)
(69 mm/yr)
(101 mm/yr)
PACIFIC
COCOS
NAZCA
km
0
20
40
60
80
100
-15°
-16°
-17°
-18°
-19°
-110°
-111°
-112°
-113°
-114°
-115°
-116°
-117°
-118°

Fig. 1a.

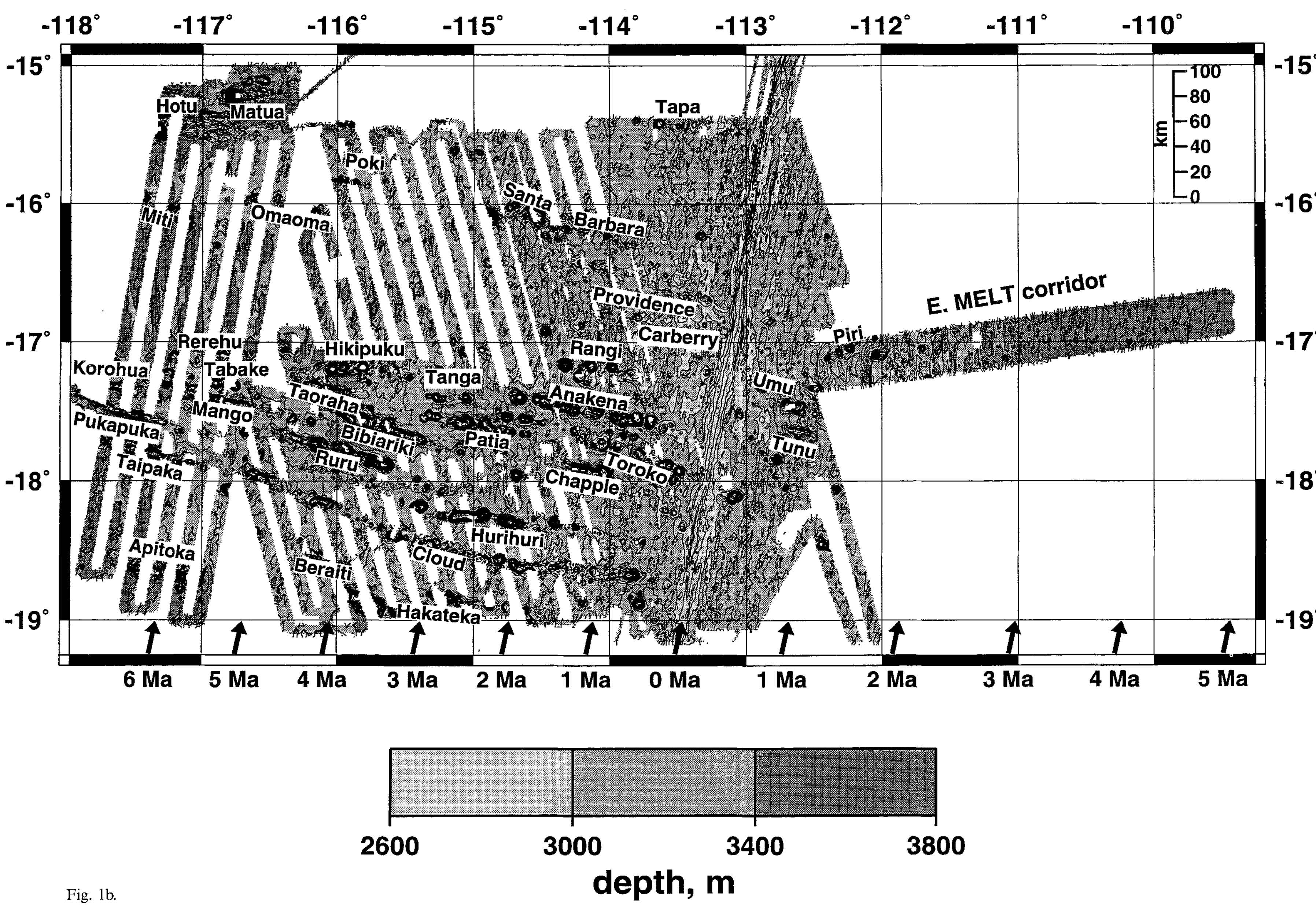

Fig. 1b.

Fig. 1. SEPR study area; inset shows the overall setting. (a) Bathymetric coverage is shaded and areas having 100% sidescan coverage are within the dashed lines. The seamounts of the Rano Rahi field are plotted as dots with their diameters scaled appropriately for the map scale. The arrows show the relative (gray) and absolute (black) plate motion vectors for the Pacific and Nazca plates. (b) 100 m contour map of the bathymetry with the seamount chain names superimposed and arrows indicating approximate seafloor ages at the bottom.

increasing distance from the axis. The Rano Rahi seamounts are associated with a number of other unusual features of this region such as significant asymmetric seafloor subsidence, asymmetric spreading, nearly collinear absolute and relative plate motion vectors on both the Pacific and Nazca plates, and the close proximity of extensive, ridge-perpendicular lineaments in the earth's gravity field (Cochran, 1986; DeMets *et al.*, 1990; Gripp and Gordon, 1990; Haxby and Weissel, 1986; Lonsdale, 1989; Naar and Hey, 1989).

The study area is centered on an 800 km-long section of the superfast spreading SEPR which is remarkably linear between the Garrett Transform Fault (~13° S) and the 20° 40' S overlapping spreading center. Between 15° and 19° S, the plate boundary is offset en echelon by a series of six very small, left-stepping, 1–5 km offset discontinuities (Figure 1a) (Lonsdale, 1989; Sinton *et al.*, 1991). Overall, spreading is significantly faster to the east by about 10–20% along this portion of the SEPR, although the degree of asymmetry is variable (Lonsdale, 1989; Mammerickx *et al.*, 1975; Naar and Hey, 1989; Perram *et al.*, 1993). At 17° S, the average Pacific spreading rate has been ~ 69 mm/yr and the average Nazca rate has been ~ 78 mm/yr since 5 Ma (D. Wilson, personal comm.). The Pacific Plate is moving significantly faster over the hot spot reference frame than is the Nazca Plate (101 mm/yr vs. 45 mm/yr) (Gripp and Gordon, 1990). The absolute and relative plate motion directions on both plates are within a few degrees of each other and are virtually ridge-perpendicular (Figure 1); the absolute plate motion directions vary by less than 3° across the entire region. These factors result in the migration of the EPR axis to the west-northwest at a rate of nearly 30 mm/yr over the hot spot frame of reference.

In most of the study area, the ridge axis is shallow, has a broad, inflated cross-section, and is the site of abundant, well-organized hydrothermal activity (Cormier and Macdonald, 1994; Renard *et al.*, 1985; Scheirer and Macdonald, 1993; Sinton *et al.*, 1991); these features are thought to indicate a robust melt supply to the axis from the upper mantle. Seismic reflection data image a strong reflection from the top of an inferred axial magma chamber which is ~1 km below the seafloor, significantly shallower than the 1.6 km depth typical of the NEPR reflector (Detrick *et al.*, 1987; Detrick *et al.*, 1993). Off-axis, the seafloor fabric is smoother and less lineated than EPR fabric elsewhere, suggesting enhanced magmatism, relative to faulting, which accommodates the seafloor spreading (Cormier *et al.*, this issue).

This area near the SEPR will receive considerable attention in the future. The results of the seamount dredging cruise, Gloria 8 (Sinton *et al.*, 1993), should provide geochemical constraints on the mantle sources of the recently erupted seamount lavas. In particular, the relationship of the Rano Rahi seamounts to an isotopic anomaly at the ridge axis (Mahoney *et al.*, 1994) is intriguing. Furthermore, the Mantle ELectromagnetic and Tomography (MELT) experiment promises to elucidate the patterns of mantle flow and melt distribution in a broad region centered on the SEPR, as well as to discern crustal structure on both sides of the ridge axis.

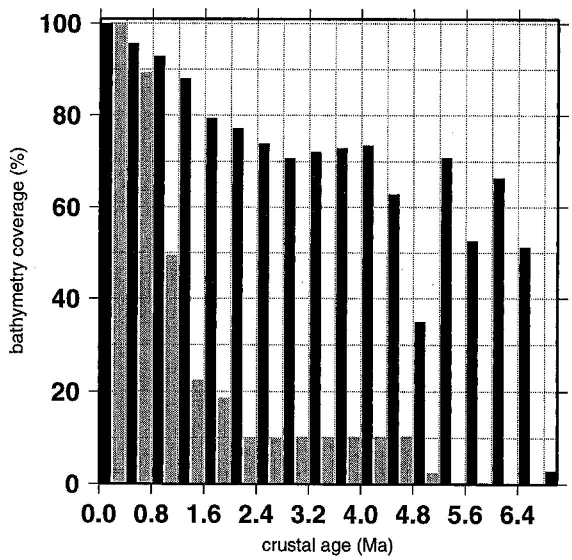

Fig. 2. Histogram of the amount of bathymetry coverage vs. crustal age. Black bars correspond to coverage on the Pacific flank, and gray bars are from the Nazca flank.

Dataset and Technique

The seamount analysis follows the development of Scheirer and Macdonald (1995) who describe the near-axis seamounts of a ~ 1000 km long section of the NEPR between 8° N and 17° N. Many of the results presented in this paper will be compared with those of the NEPR, which is the only other study with comparable off-axis coverage near a fast spreading center.

Four major swath-mapping cruises mapped the flanks of the SEPR between 15° S and 19° S: legs 2 and 3 of the Gloria expedition aboard the Melville in 1992–1993, Rapa leg 2 aboard the Washington in 1990–1991, and MW8710 aboard the Moana Wave in 1987. These cruises variously collected swaths of SeaBeam2000 (Gloria 2 and 3), SeaMARCII (MW8710 and Rapa 2), HMR1 (Gloria 2), and Seabeam (Rapa 2) bathymetry data as well as HMR1, SeaMARCII, and SeaBeam2000 sidescan. The combined survey yields complete bathymetry and sidescan coverage from the ridge axis out to nearly 90 km on both flanks, with 50% bathymetry and nearly 100% sidescan coverage continuing as far as 470 km on the western flank (Figure 2). On the eastern flank, a 40 km-wide, 300 km-long corridor was surveyed for the MELT experiment (Figure 1). The 100% bathymetry coverage extends to the Jaramillo Anomaly (~ 1 Ma) on both flanks, and the 50% coverage reaches nearly 6.5 Ma on the Pacific flank. The MELT corridor extends to seafloor aged just over 4.5 Ma. The total area of bathymetry coverage is slightly greater than 200,000 km^2, comparable to that of the well-surveyed flanks of the NEPR (Macdonald *et al.*, 1992), and the data provide an ideal overview of the seafloor morphology, as imaged from the sea surface, created by the superfast spreading center.

Most of the seamounts were identified and measured at-sea during the Gloria legs, on SeaBeam2000 real-time swath bathymetry records contoured at 20 m. Included in the seamount tally were any local highs having more than 100 m of relief within closed contours of aspect ratio less than two. Extensive editing of the initial seamount picks to include edifices on the edges of swaths, to correct for seamounts counted more than once, and to incorporate seamounts surveyed during Rapa 2 and MW8710 yielded our final seamount tabulation. The bathymetry data from all of the cruises were gridded at 200 m spacing, contoured every 50 m in depth, and plotted at a UTM scale of 1:400,000 which co-registers with sidescan mosaics. Because of the less precise bathymetry derived from the SeaMARCII system (Macdonald *et al.*, 1992), only seamounts ≥ 200 m tall were counted for the Rapa and MW8710 surveys, and these were picked from the 50 m contour interval basemaps. Thus, for seamount analyses which require accounting for the entire population of seamounts from given regions, we restrict our consideration to those seamounts 200 m and taller. Also, because during much of Gloria 3 we preferentially surveyed seamounts in the central part of the study area, we omit the Gloria 3 coverage from areal distribution analyses to avoid biasing the resulting seamount abundance estimates.

For each seamount, we tabulate the position of its center, its basal depth, its height (above the base), its basal diameter (if non-circular, the average diameter), the diameter of any summit plateau, the seamount's distance from the ridge axis, and any significant morphologic features, such as the presence of a summit depression or its belonging to a seamount chain. Based on these measurements and by approximating the seamounts as truncated, right circular cones, we estimate the volume, flatness (summit diameter divided by basal diameter), and average flanking slope of each tabulated edifice. The table of Rano Rahi measurements is available via anonymous ftp, as described in the Appendix. In a number of locations in the western part of the survey, the seamount chains consist of overlapped volcanoes and volcanic ridges which are not amenable to this classification scheme. While we approximate these features as overlapped cones to include in our table for completeness, we restrict our analyses of individual edifices to those seamounts on crust younger than 5 Ma to avoid the presence of the ridges. We also estimate the volume of the seamount edifices using gridded bathymetry and the areally anisotropic median filtering technique of Shen *et al.* (1993); this method effectively separates out the topography that one would visually identify as belonging to seamounts from the surrounding seafloor.

General Observations

We tabulated 1105 seamounts ≥ 100 m high in the 200,300 km^2 area of bathymetry coverage. About 250 similar-sized seamounts occur in the additional ~ 40,000 km^2 where there is only sidescan coverage. The total number of seamounts ≥ 200 m tall on both flanks is 646, and disregarding those from Gloria 3, these seamounts have an average abundance (number of seamounts per area of bathymetry coverage) of 2.9 smts/1000 km^2. This is nearly three times the value of 1.1 smts/1000 km^2 for the NEPR (Scheirer and Macdonald, 1995). Most of the observed seamounts are on the Pacific flank, in large part due to its greater amount of coverage. On the Pacific Plate, the seamounts are not distributed uniformly as there are twice as many ≥ 200 m tall seamounts south of 17° S (4.4 smts/1000 km^2) as there are to the north (2.2 smts/1000 km^2).

The available data (Figure 1) are ambiguous as to whether the seamounts are symmetrically distributed about the SEPR. South of 18° 10' S, there are many more ≥ 200 m edifices on the young Pacific Plate than on equivalently aged Nazca Plate (which has only one small seamount). North of 18° 10' S, the numbers of seamounts on crust < 1 Ma are approximately equal. The only major portion of the survey extending to older ages on the Nazca flank has few seamounts, but this Eastern MELT corridor reflects about the axis of the SEPR to an area of the Pacific Plate which is also nearly devoid of seamounts (Figure 1). Pre-existing ship profiles are very sparse, but do show some (but

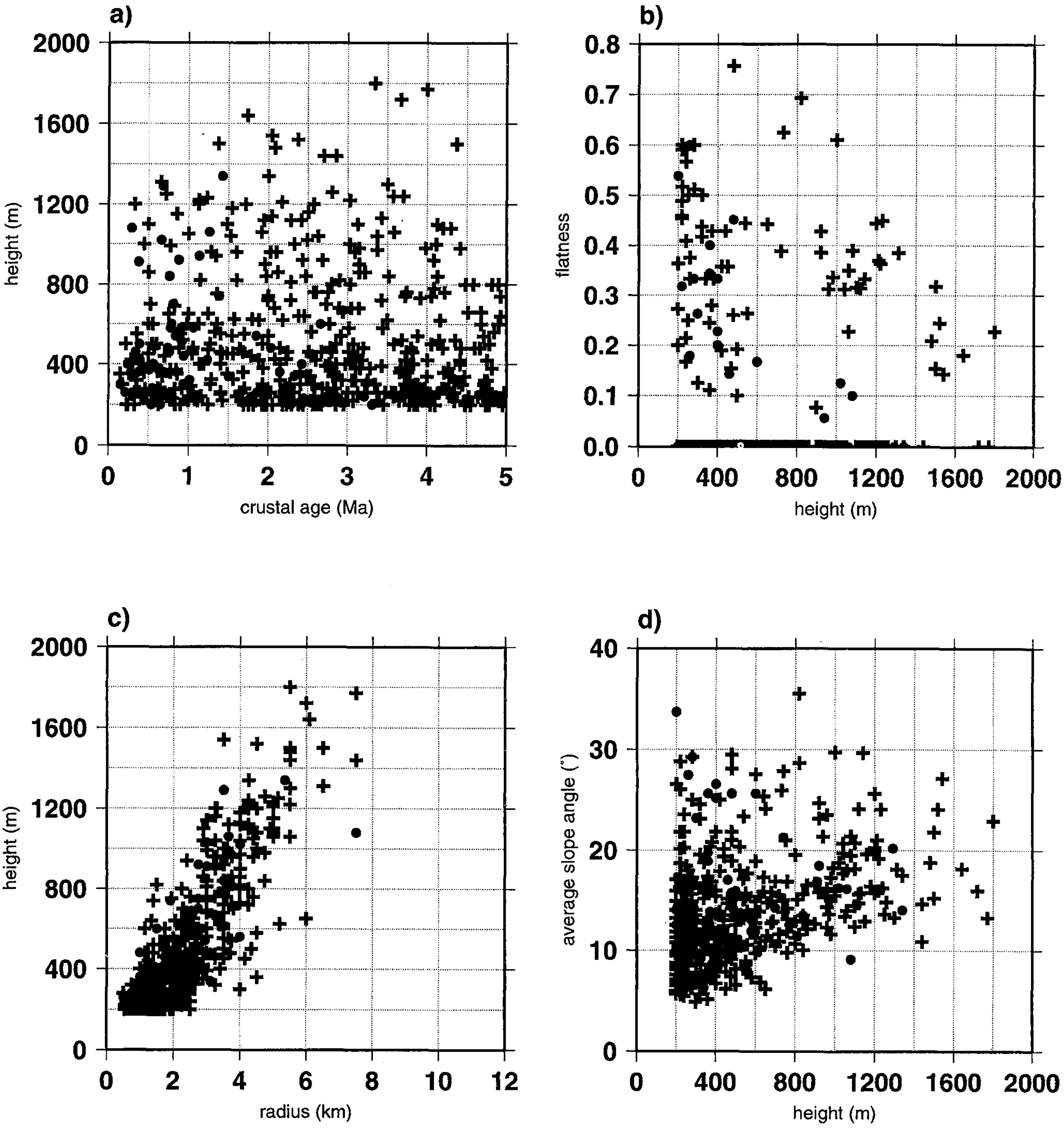

Fig. 3. Properties of the SEPR seamounts which are taller than 200 m and which lie on crust younger than 5 Ma. Crosses indicate seamounts on the Pacific Plate; filled circles represent Nazca seamounts. (a) displays the rapid growth in abundance and size of the seamounts very near the axis. Flatness, (b), is the ratio between the diameter of any summit plateau to the diameter of the seamount's base; 80% of the seamounts have no discernible plateau (zero flatness). (c) plots seamount heights vs. their basal radii. The average slope angle, (d), is determined by approximating the seamounts as truncated cones.

not many) seamount edifices on the Nazca flank.

The majority of seamounts in our survey area are several hundred meters high, have diameters of several kilometers, and have pointy to relatively flat tops. A number of these properties are displayed in Figure 3 for seamounts on crust aged < 5 Ma (where most of the edifices can be well-approximated by cones). These characteristics of the SEPR seamounts are similar to

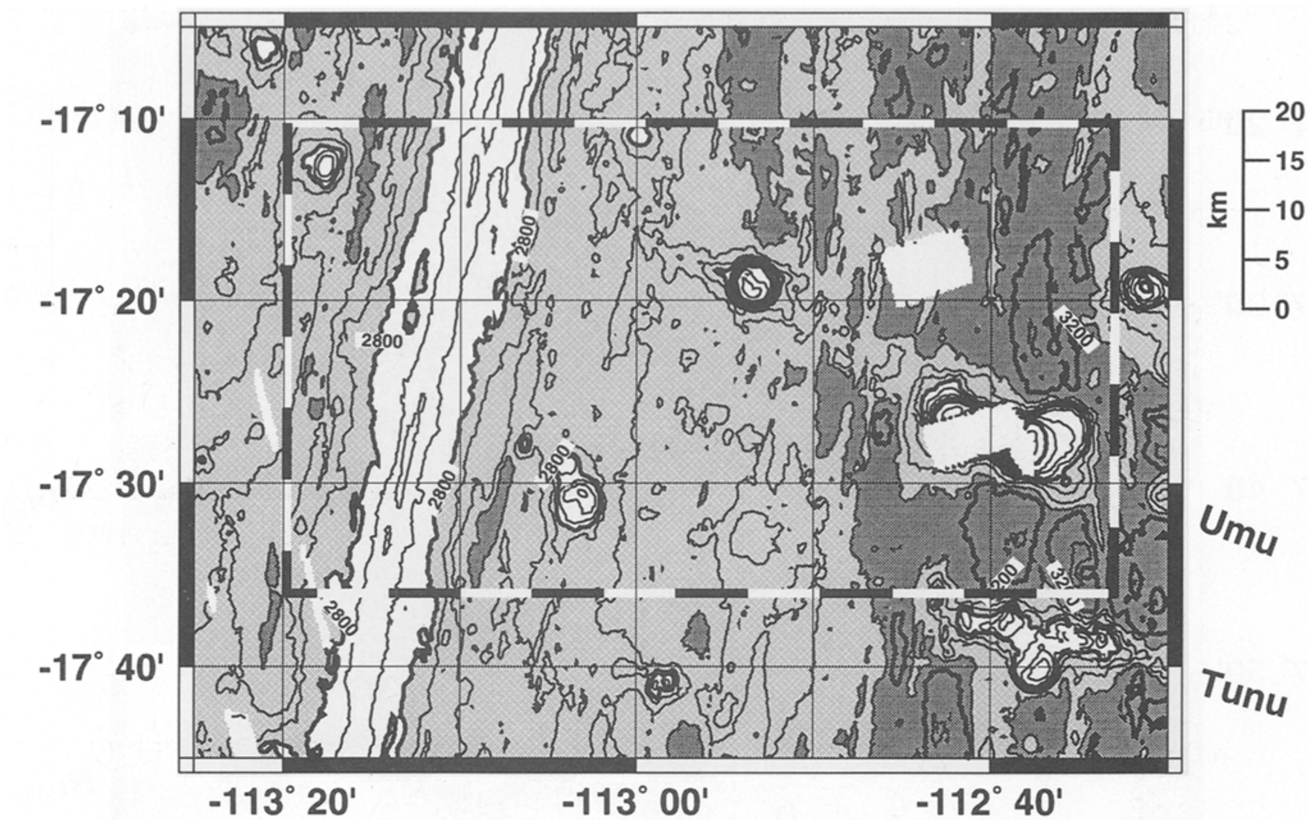
-17° 10'
-17° 20'
-17° 30'
-17° 40'
2800
3200
km
20
15
10
5
0
Umu
Tunu
-113° 20'
-113° 00'
-112° 40'

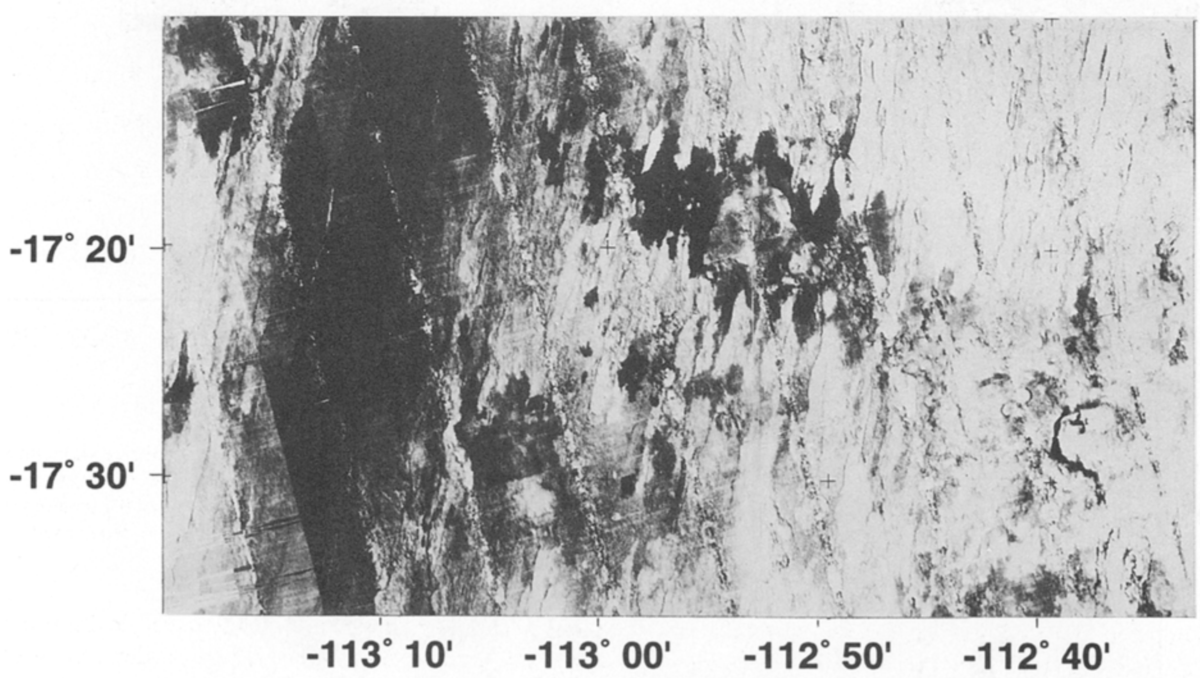
-17° 20'
-17° 30'
-113° 10'
-113° 00'
-112° 50'
-112° 40'

Fig. 4a.

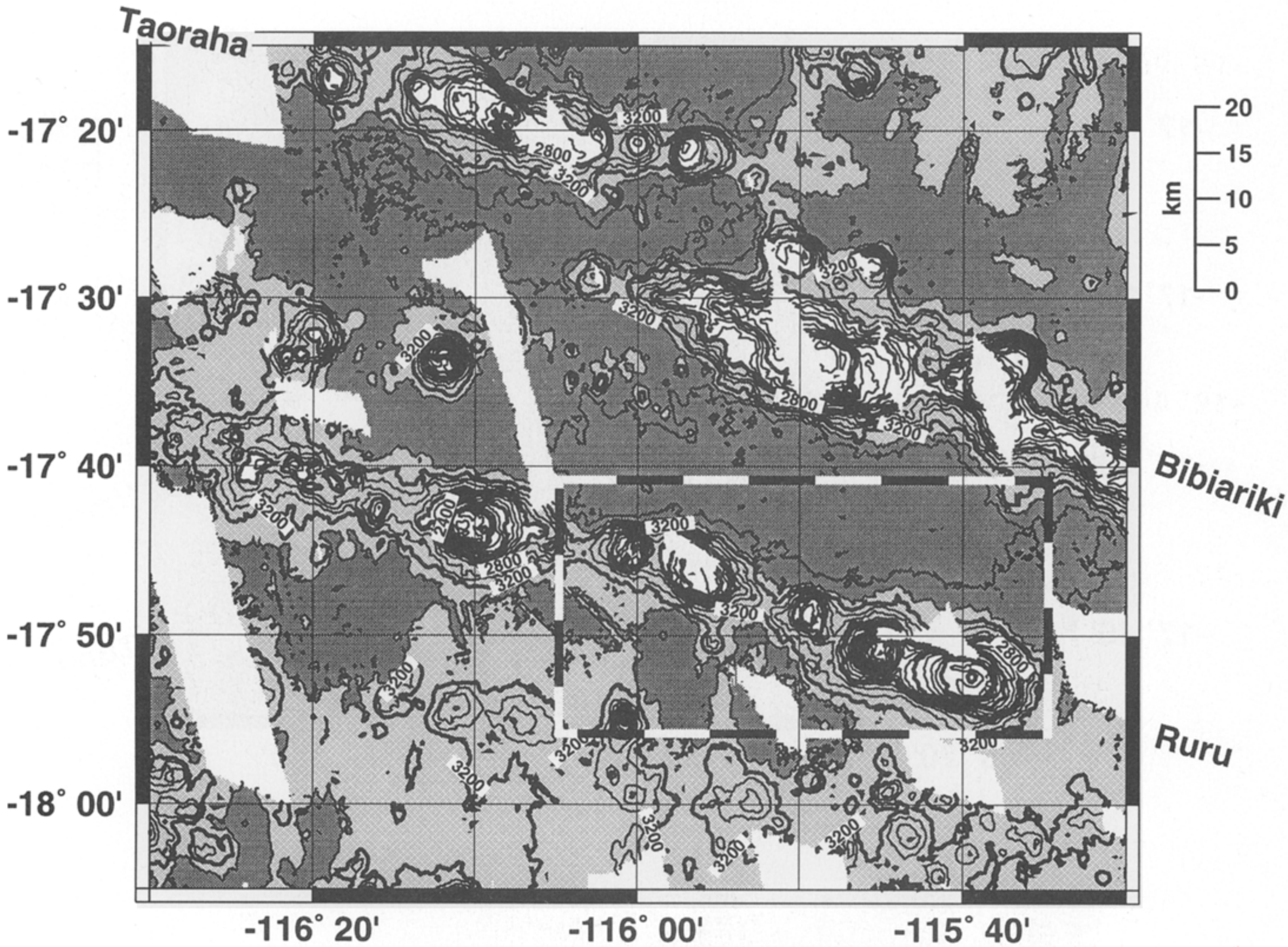
Taoraha
Bibiariki
Ruru
-17° 20'
-17° 30'
-17° 40'
-17° 50'
-18° 00'
-116° 20'
-116° 00'
-115° 40'
km
20
15
10
5
0
3200
2800

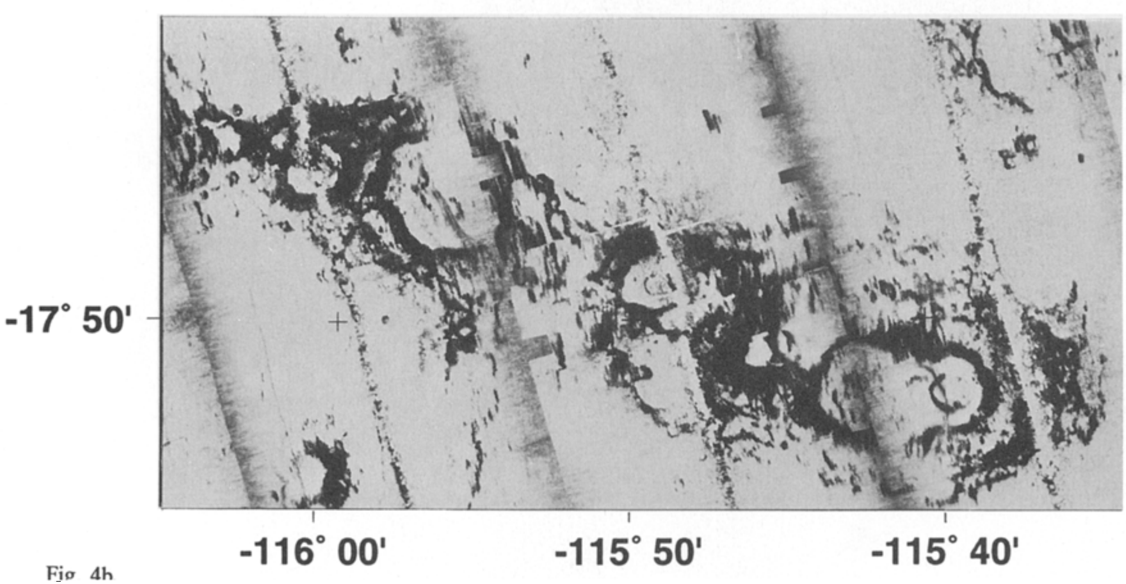
-17° 50'
-116° 00'
-115° 50'
-115° 40'

Fig. 4b

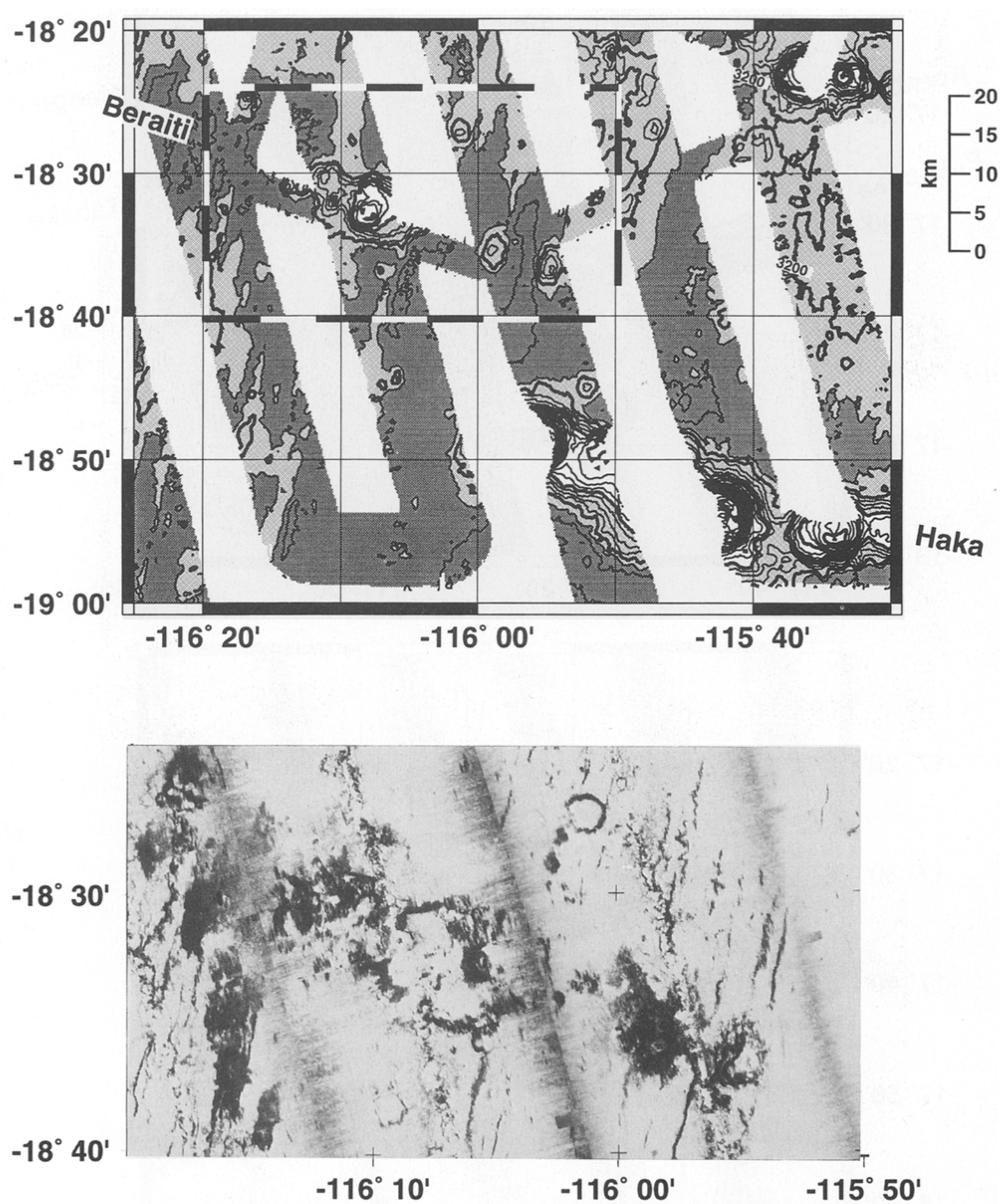
-18° 20'
-18° 30'
-18° 40'
-18° 50'
-19° 00'
-116° 20'
-116° 00'
-115° 40'
Beraiti
Haka
3200
3200
km
20
15
10
5
0
-18° 30'
-18° 40'
-116° 10'
-116° 00'
-115° 50'

Fig. 4c.

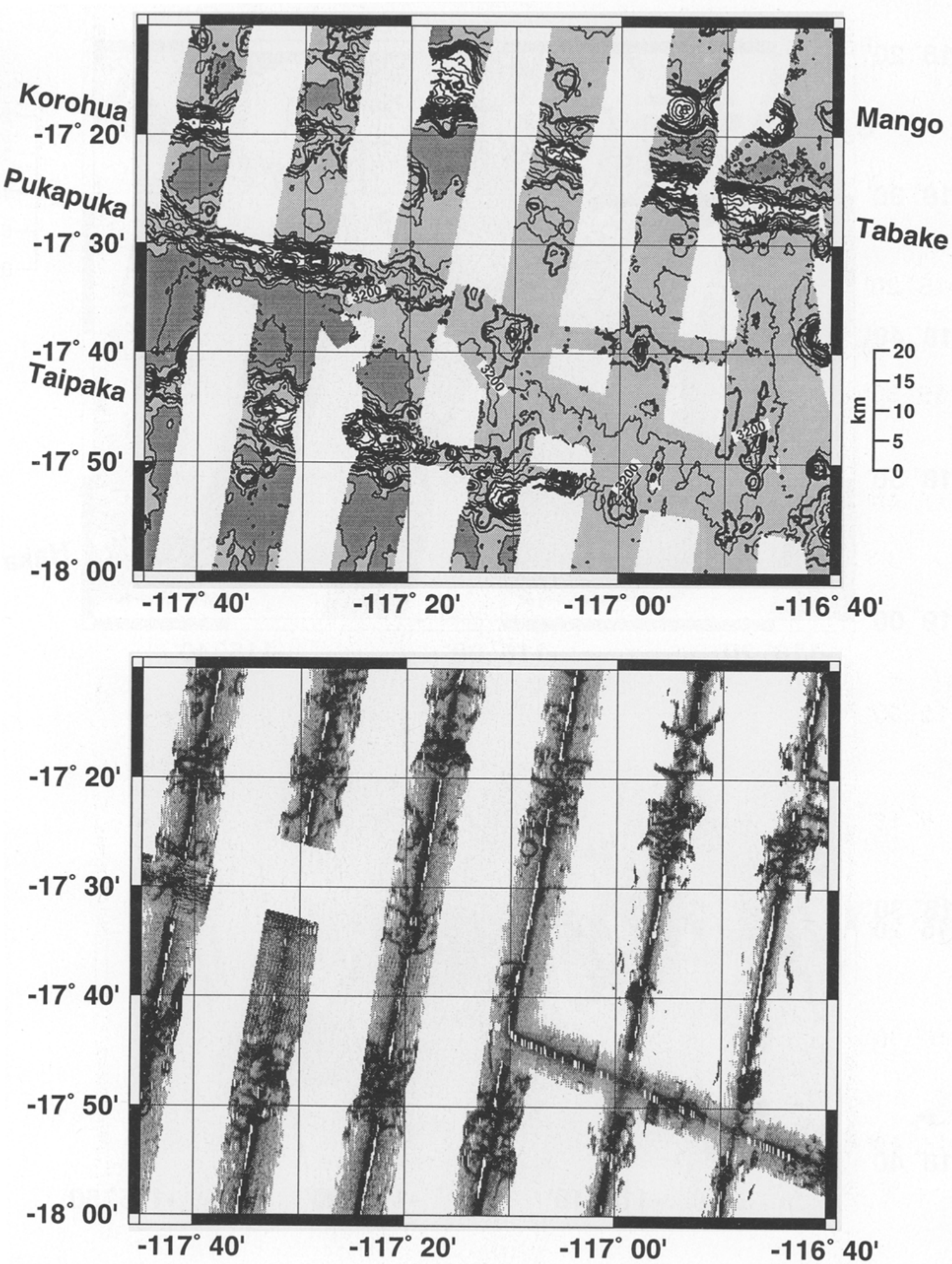
Korohua
-17° 20'
Pukapuka
-17° 30'
-17° 40'
Taipaka
-17° 50'
-18° 00'
Mango
Tabake
3200
km
20
15
10
5
0
-117° 40'
-117° 20'
-117° 00'
-116° 40'
-17° 20'
-17° 30'
-17° 40'
-17° 50'
-18° 00'
-117° 40'
-117° 20'
-117° 00'
-116° 40'

Fig. 4d.

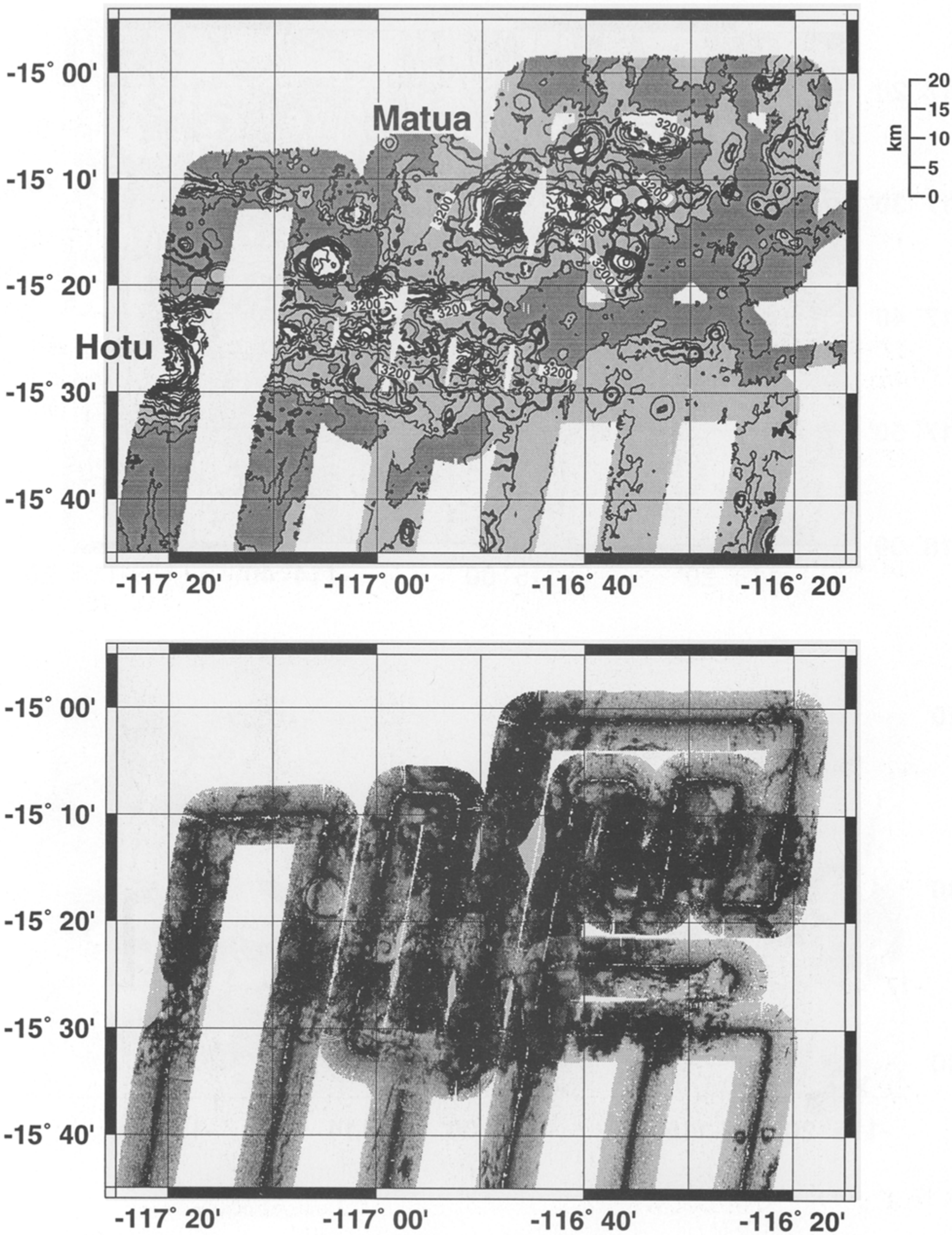
-15° 00'
-15° 10'
-15° 20'
-15° 30'
-15° 40'
Matua
Hotu
3200
km
20
15
10
5
0
-117° 20'
-117° 00'
-116° 40'
-116° 20'
-15° 00'
-15° 10'
-15° 20'
-15° 30'
-15° 40'
-117° 20'
-117° 00'
-116° 40'
-116° 20'

Fig. 4e.

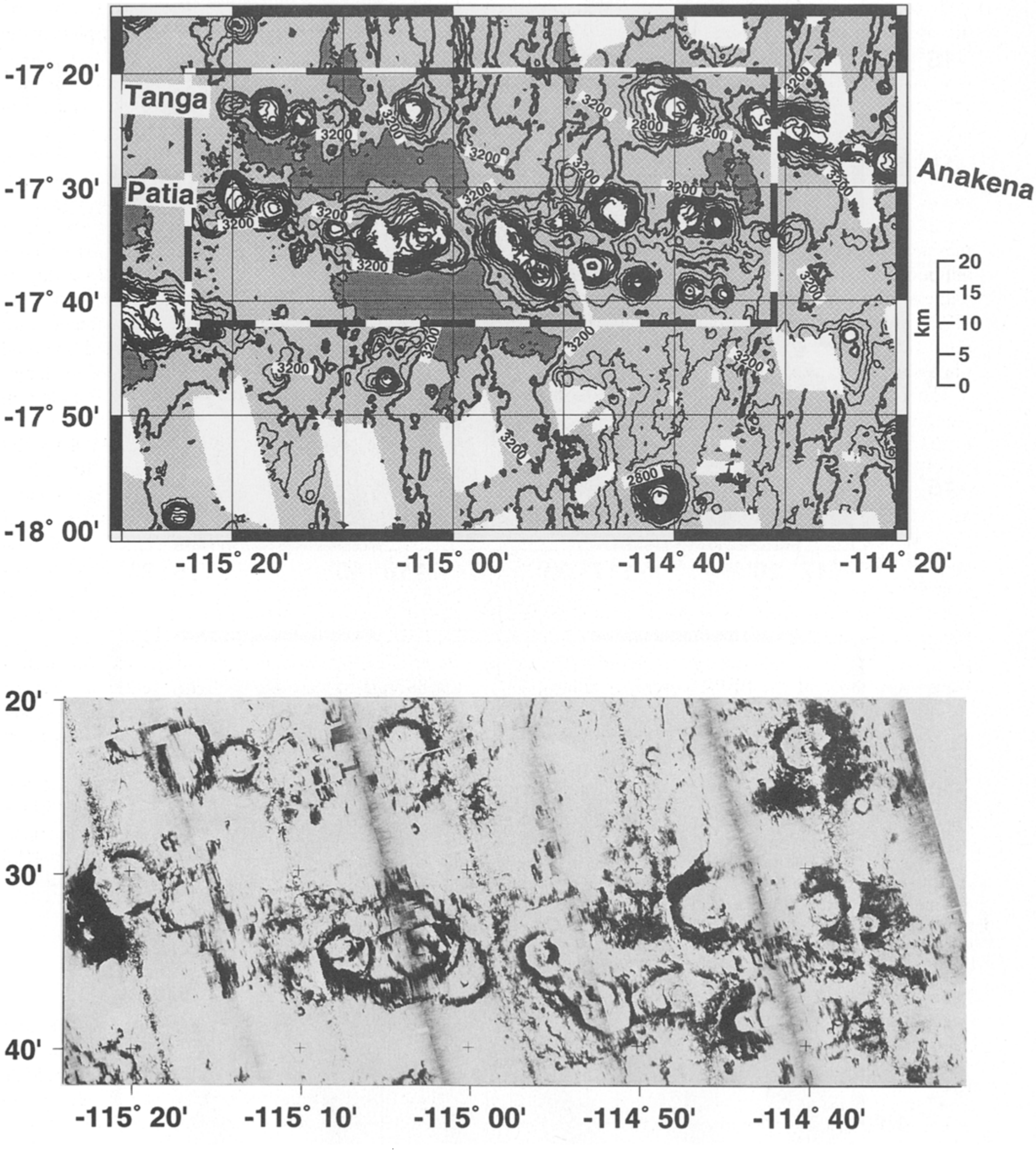
-17° 20'
-17° 30'
-17° 40'
-17° 50'
-18° 00'
-115° 20'
-115° 00'
-114° 40'
-114° 20'
Tanga
Patia
Anakena
3200
2800
km
20
15
10
5
0
-115° 10'
-114° 50'

Fig. 4f.

their counterparts near the NEPR. In general, there are no observable differences in the character of the Pacific and Nazca seamounts other than their relative abundance. As along the NEPR, there are no edifices on the axis itself, but large seamounts (> 1000 m high) occur on plate of young ages (<0.5 Ma), Figure 3a. There is a small increase in the observed maximum seamount height out to 3.5 Ma. Flatness, Figure 3b, ranges between 0 and 0.75 with a tendency for smaller maximum flatness values for the taller edifices. The minimum non-zero flatness we can estimate is ~ 0.1, and most of the seamounts (80%) have no measurable flatness. The minimum measurable flatness of the NEPR study (Scheirer and Macdonald, 1995) is ~ 0.2, due to the coarser contour interval, 50 m, which did not allow for the recognition of small summit plateaus.

The typical height to radius ratio for the SEPR seamounts, Figure 3c, is 0.20, slightly higher than that of the NEPR (0.17) but comparable to other surveys (Smith, 1988). The scatter about this average ratio is significant and, combined with the variability in flatness values, brings about the wide variability in average slope values, Figure 3d; these fall mostly between 5° and 30°. The greater height/radius ratio of the SEPR seamounts results in steeper slopes than those of the NEPR edifices, especially for seamounts smaller than 600 m. These differences may be explained, in large part, by the finer bathymetry resolution of SeaBeam2000 (most of the SEPR coverage) relative to SeaMARCII (most of the NEPR coverage), which resolves steeper slopes and smaller summit plateaus in the Rano Rahi Field.

Figure 4 presents bathymetry and sidescan data from six areas to illustrate the map-view characteristics and variability of these seamounts. Figure 4a displays a portion of the ridge axis and a number of seamounts forming on the Nazca flank; they are surrounded by high reflectivity lava flows. Figure 4b shows a dense assemblage of seamount chains near the center of the seamount field. The large chains are composed of individual cones which overlap at their bases. The deep, unlineated areas result from flexural down warping of the plate combined with in-filling of lava flows and mass-wasted material which obscures the abyssal scarps. Many of the larger edifices have distinctly flat tops and small craters in the sidescan image.

Figure 4c displays the Haka chain and the small Beraiti chain with its highly reflective lava flows bounded by abyssal scarps. Figure 4d presents a number of the volcanic ridges in the westernmost portion of the survey, situated on crust older than 5 Ma. Although there are a few isolated and overlapped edifices, the main form of volcanic construction in this area is lineated. Figure 4e displays the complex volcanic cluster, Hotu Matua, in the north-westernmost corner of our survey. The edifices lie mainly in two, sub-parallel clusters elongated east-west. Highly reflective seafloor covers an area >3900 km^2 surrounding all of the edifices. Figure 4f shows the Patia chain which appears to split at 114° 55' W.

An alternate view of seamount morphology is presented in Figure 5 as perspective views of the "Three Wisemen", near the center of the Hurihuri chain. These edifices range in height from 1100 m to 1500 m, and each has a significant crater between 50 m and 140 m deep.

Fig. 4. Examples of SEPR seamount bathymetry (top) and sidescan (bottom) data. The bathymetry, derived primarily from SeaBeam2000 measurements, is contoured at 100 m with heavy lines and annotation every 400 m. Gray-shading in each case highlights the locations of deep and shallow seafloor; the numbers in parentheses for each figure indicate the depths in meters at which the shading changes from dark gray to light gray and from light gray to white. Dashed boxes indicate the locations of the displayed sidescan data. The sidescan panel displays HMR1 data, unless otherwise noted. Dark returns indicate strong backscatter such as from unsedimented seafloor or steep slopes. (a) (3100/2800) A portion of the SEPR axis and a number of recently active seamounts. Note how the seafloor reflectivity decreases rapidly within 15 km of the axis. The distal edges of many off-axis flows are bounded by abyssal scarps. (b) (3300/2800) A dense area of seamount chains centered ~ 300 km west of the axis. The seafloor is deeper around the largest chains due to flexure of the plate from seamount loading. (c) (3300/2800) The large Haka chain along with the small Beraiti chain which has fresh volcanism ~ 280 km from the axis (on crust ~ 4 Ma). (d) (3400/2800) Volcanic ridges in the westernmost portion of the survey (~ 450 km from the axis). The sidescan data are from the SeaBeam2000 system 4-bit output and are gridded at 200 m. (4) (3400/2800) The Hotu Matua seamounts in the northwest corner of the survey display widespread, fresh volcanism in the SeaBeam2000 sidescan. (f) (3300/2800) The Patia seamount chain which splits in two, ~ 170 km west of the axis.

Seamount Size Distribution

To quantify the size distribution of seamounts, Jordan *et al.* (1983) and subsequent studies consider the cumulative number of seamounts having heights greater than a certain value. Empirically, this relationship takes the form of a negative exponential distribution over a large range of seamount heights. Adopting the nomenclature of Smith and Jordan (1987), this distribution is expressed as: $\nu(H) = \nu_0 * \exp(-\beta H)$, where $\nu(H)$ is the number of seamounts per unit area having height greater than H, ν_0 is the total number of seamounts per unit area, and β is the

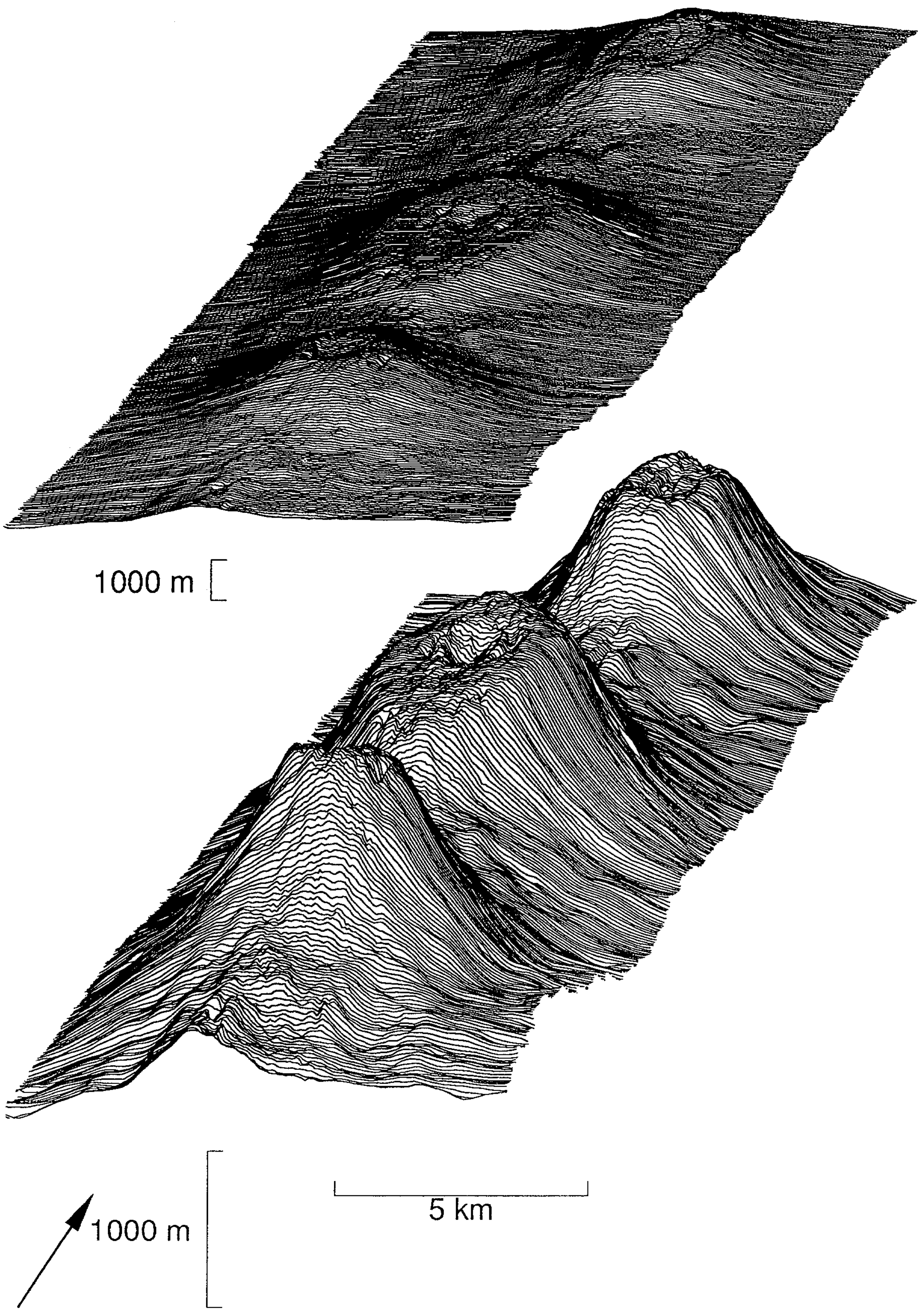

Fig. 5. Perspective views of the "Three Wisemen" in the Hurihuri chain, from a single SeaBeam2000 swath oriented at 98°. View is looking to the northeast, and the central volcano is located at 18° 18' S, 114° 43' W. Vertical exaggerations are 1 (top) and 4 (bottom).

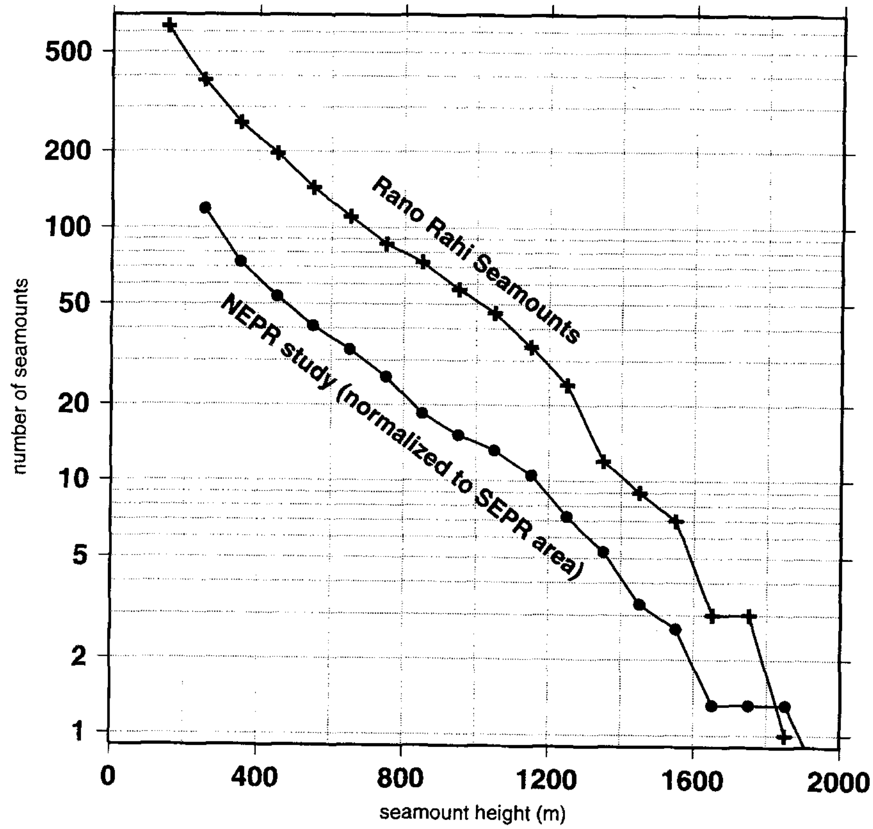

Fig. 6. The cumulative number of SEPR seamounts on crust <5 Ma, +, in the 132,000 km^2 of bathymetry coverage which is not biased by lines running along seamount chains. The circles are the corresponding data from the NEPR seamounts (Scheirer and Macdonald, 1995), correcting the NEPR values for the difference in area between the studies.

negative of the slope of a line fitting ln(ν(H)) vs. H. The reciprocal of β yields a characteristic height of the seamount sample. A plot of ln(ν(H)) versus H is shown in Figure 6. The cumulative distribution of seamounts on crust <5 Ma is fairly linear over the size range from 200–1200 m. A maximum likelihood fit (Smith and Jordan, 1987) to the distribution in this range yields $\nu_0 = 4.8$ smts/1000 km^2, $\beta = 2.4$ /km, and a characteristic height of 420 m. Table I compares these values with those from other studies (Abers *et al.*, 1988; Bemis and Smith, 1993; Kleinrock *et al.*, 1994; Scheirer and Macdonald, 1995; Smith and Cann, 1992; Smith and Jordan, 1987). The slope of the regression, $-\beta$, is distinct from that of the NEPR study, and the cumulative abundance of the Rano Rahi seamounts is over three times as great in this size range (Figure 6). Of the other prior studies in Table I, the results of Smith and Jordan (1987) from the East Pacific are most similar to the results from the Rano Rahi area; these studies also share the most comparable ranges of seamount size.

Seamount Chains and Volcanic Ridges

More than 75% of the seamounts in the study area belong to one of about 35 seamount chains and volcanic ridges. In the following discussion, we will include volcanic ridges in the following broad definition of seamount chains in this area: any off-axis, lineated, genetically-related volcanic construction and groups of edifices. The properties of the seamount chains are summarized in Table II. We have given most of these seamount chains names in Pascuense (Figure 1b), the language of Rapa Nui, in recognition of our port calls at Easter Island and in honor of the first sailors to navigate these waters. Other chains were named from earlier cruises (e.g. Shen *et al.* (1993)). We have submitted the Rano Rahi designation and the names of 14 of the largest chains to the International Hydrographic Organization in Monaco for consideration as additions to the GEBCO Gazetteer (Table II).

The seamount chains range in length from ~ 25 km to more than 240 km, and the Cloud chain may be as

TABLE I
Seamount size distribution parameters, $\nu = \nu_0 \exp(-\beta H)$

Study	Area	Height range (m)	β (1/km)	ν_0 (/1000 km^2)	characteristic height (m)	predicted # for 132,000 km^2 ≥300m	≥500m
This study[1]	SEPR	200–1200	2.4 ± 0.1	4.8 ± 0.3	421	308	191
Scheirer & Macdonald (1995)	NEPR	200–800	4.3 ± 0.2	1.9 ± 0.2	235	69	29
Abers *et al.* (1988)[2]	S.Pacific	100–600	12.9 ± 2.5	27.2 ± 8.6	80	75	6
Bemis & Smith (1993)[3]	S.Pacific	50–210	15.9 ± 0.6	33.0 ± 2	63	37	2*
Smith & Jordan (1987)[4]	E.Pacific	400–2500	3.5 ± 0.2	5.4 ± 0.7	290	249*	123
Kleinrock *et al.* (1994)	Galapagos	50–350	34.5 ± 2.5	370 ± 30	29	2	$\ll 1$*
Smith & Cann (1992)	N.MAR	50–210	17.2 ± 0.5	195 ± 0.9	60	148*	5*
Observed number of seamounts in 132,000 km^2 SEPR study area:						260	143

[1] Pre-Gloria 3 seamounts only.
[2] 0–2 Ma region.
[3] EPR region.
[4] All areas.

* Predicted number of seamounts for this size is outside the height range of the study.

long as 350 km. The median chain length is 62 km. Where composed of distinct edifices, the chains contain from 3 to >25 volcanoes taller than 200 m. Where more ridge-like, they are typically ~ 50 km long, 1000–1500 m high, shallowest in their centers, and gradually tapered towards their ends. Figure 7 displays the along-ridge relief and volume variation for three volcanic ridges in the westernmost portion of the survey. Although the data coverage is incomplete, they clearly differ in slope and volume variation from the Ruru chain of overlapped seamounts (Figures 7 and 4b). The along-ridge slopes of these volcanic ridges are many times greater than the along-axis slopes of intermediate and fast spreading centers; however, the along-axis slopes of the slow-spreading Mid-Atlantic Ridge are comparable to the Rano Rahi volcanic ridges. Small, circular edifices sometimes lie atop the volcanic ridges, but the main volume is contained within the high aspect-ratio contours. These types of ridges are similar to, but generally smaller than, the series of volcanic ridges which extends along the Pukapuka Ridge System from the western edge of our survey more than 2500 km to the west-northwest (Sandwell *et al.*, submitted).

At their closest spacing, the seamount chains are separated by 15–20 km between their axes. They vary significantly in volume both along individual chains and among different chains. In some cases, it is ambiguous whether separated but collinear groups of seamounts are part of the same chain.

Most of the seamount chains form single, linear segments although several of the Pacific chains are composed of multiple segments separated by bends of between 6° and 15° (Table II). Of the six significant bends, half bend to the right approaching the axis and half bend to the left. The latter sense of re-orientation, becoming more east-west towards the axis, is most striking in the Cloud and Hurihuri chains which have long segments at distinct orientations (Figure 1b). A single plate motion change cannot account for these different senses of rotation, and the absence of direction changes along most of the chains suggests that their cause is related to changes in the location of the melt source and/or the path that magma ascends to the seafloor.

The orientations of the Pacific chains, Figure 8, fall very close to the best-fit plate motion directions of NUVEL-1 and HS-NUVEL-1 (DeMets *et al.*, 1990; Gripp and Gordon, 1990), which are indistinguishable on the Pacific Plate. The Pacific seamounts cluster symmetrically within 10° of the 282° motion direction. This clustering is much stronger than that observed for the seamount chains of the NEPR (Scheirer and Macdonald, 1995), where the absolute and relative plate motion directions for both the Pacific and Cocos plates are separated by 20° or more.

Some of the SEPR seamount chains exhibit a plan geometry which deviates significantly from the piecewise continuous line segments of the majority of chains. The Patia seamount chain, Figure 4f, splits into two nearly equal-sized, parallel lines of seamounts

TABLE II
Rano Rahi seamount chains

Name	Pac/ Naz	lat-lon (west end)		lat-lon (east end)		Length (km)	Orientation (° ± °)		# smts	Pascuense meaning	
Haka	P	18° 48′	115° 58′	18° 59′	115° 15′	83	283	3	6+	endless-	*
Haka-W	P	18° 48′	115° 58′	18° 53′	115° 42′	27	287	3	3+		
Haka-E	P	18° 53′	115° 42′	18° 59′	115° 15′	54	276	3	3+		
Teka	P	18° 47′	115° 19′	18° 56′	114° 31′	86	280	2	7+	corners	*
Beraiti	P	18° 30′	116 °12′	18° 36′	115° 55′	33	288	2	5+	little fire	
Apitoka	P	18° 36′	117° 40′	18° 43′	117° 01′	72	281	2	3+	fresh lava	*
Cloud	P	18° 20′	115° 42′	18° 44′	113° 32′	210	285	10	25+	**	*
Cloud-W	P	18° 20′	115° 42′	18° 37′	114° 40′	95	286	3	15+		
Cloud-E	P	18° 37′	114° 40′	18° 44′	113° 32′	116	274	3	10+		
Hurihuri	P	17° 53′	116° 17′	18° 26′	113° 46′	242	282	10	20+	incessant rolling	*
Hurihuri-W	P	17° 53′	116° 17′	18° 15′	115° 14′	110	287	4	10+		
Hurihuri-M	P	18° 15′	115° 14′	18° 22′	114° 28′	79	275	2	6+		
Hurihuri-E	P	18° 18′	114° 24′	18° 26′	113° 46′	55	282	2	4+		
Chapple	P	17° 55′	114° 23′	17° 57′	114° 03′	39	277	3	3	***	*
Toroko	P	17° 37′	114° 16′	17° 55′	113° 29′	94	289	2	8+	wild grasses	*
Anakena	P	17° 19′	114° 40′	17° 37′	113° 28′	134	282	1	15+	Rapa Nui beach	*
Rangi	P	17° 08′	114° 21′	17° 13′	113° 50′	62	278	2	5	sky	*
Patia	P	17° 31′	115° 23′	17° 41′	114° 34′	97	279	2	18+	fork	*
Patia-N	P	17° 32′	114° 46′	17° 35′	114° 29′	40	279	2	5+		
Patia-S	P	17° 31′	115° 23′	17° 41′	114° 34′	97	279	2	14+		
Tanga	P	17° 23′	115° 22′	17° 23′	115° 02′	39	272	3	4	youth	
Ruru	P	17° 39′	116° 25′	17° 52′	115° 37′	94	287	3	8+	shake	*
Bibiariki	P	17° 28′	116° 03′	17° 46′	115° 17′	86	289	2	4	king of chains	*
Taoraha	P	17° 16′	116° 04′	17° 21′	115° 57′	48	282	2	5	whale	
Hikipuku	P	17° 10′	116° 10′	17° 12′	115° 15′	99	273	4	9+	to boast an error	
Taipaka	P	17° 43′	117° 46′	17° 56′	117° 12′	72	287	3	R	calm seas	*
Pukapuka	P	17° 27′	117° 46′	17° 37′	117° 11′	95	283	2	R	****	
Mango	P	17° 13′	117° 28′	17° 27′	116° 40′	84	288	6	R	shark	
Tabake	P	17° 14′	117° 05′	17° 24′	116° 36′	35	281	3	5+	sea-bird	
Korohua	P	17° 20′	117° 42′	17° 25′	117° 19′	44	281	3	R	ancient	
Rerehu	P	17° 06′	117° 15′	17° 11′	116° 39′	68	276	4	5	collapse	
Miti	P	15° 57′	117° 27′	16° 08′	117° 06′	46	296	6	3	sediment	
Omaoma	P	15° 57′	116° 37′	16° 04′	116° 09′	59	282	4	3	meager	
Hotu	P	15° 27′	117° 20′	15° 30′	116° 43′	70	270	8	8+	legendary	*
Matua	P	15° 13′	116° 51′	15° 13′	116° 27′	57	269	5	5+	leader	*
Poki	P	15° 48′	116° 02′	15° 51′	115° 47′	28	284	2	3	child	
Carberry	P	16° 50′	113° 55′	16° 52′	113° 12′	77	275	4	6		
Carberry-W	P	16° 50′	113° 55′	16° 49′	113° 27′	50	270	2	2		
Carberry-E	P	16° 49′	113° 27′	16° 52′	113° 12′	28	281	2	4		
Providence	P	16° 25′	114° 13′	16° 43′	113° 09′	123	278	4	9+		
Providence-W	P	16° 25′	114° 13′	16° 29	113° 46′	61	277	2	4+		
Providence-E	P	16° 35′	113° 41′	16° 43	113° 09′	62	281	2	5		
Santa	P	16° 04′	114° 48′	16° 10′	114° 20′	66	282	6	9+		
Santa-W	P	16° 04′	114° 48′	16° 04′	114° 32′	38	272	6	4+		
Santa-E	P	16° 04′	114° 32′	16° 10′	114° 20′	27	287	6	4+		
Barbara	P	16° 14′	114° 03′	16° 16′	113° 51′	29	281	3	5		
Tapa	P	15° 23′	113° 49′	15° 24′	113° 05′	79	272	3	9+	edge	
Piri	N	17° 06′	112° 25′	16° 56′	112° 03′	46	068	4	5+	riddle	
Umu	N	17° 17′	112° 58′	17° 30′	112° 30′	57	121	6	4	oven	
Tunu	N	17° 36′	112° 44′	17° 40′	112° 30′	26	105	3	5	cooking	

W – western segment; E – eastern segment; N – northern segment; S – southern segment; M – middle segment; R – volcanic ridge.
* Name submitted to the International Hydrographic Organization.
** Named for Preston Cloud.
*** Named for William Chapple.
**** Named for Pukapuka Island (in eastern Tuamotu Archipelago).

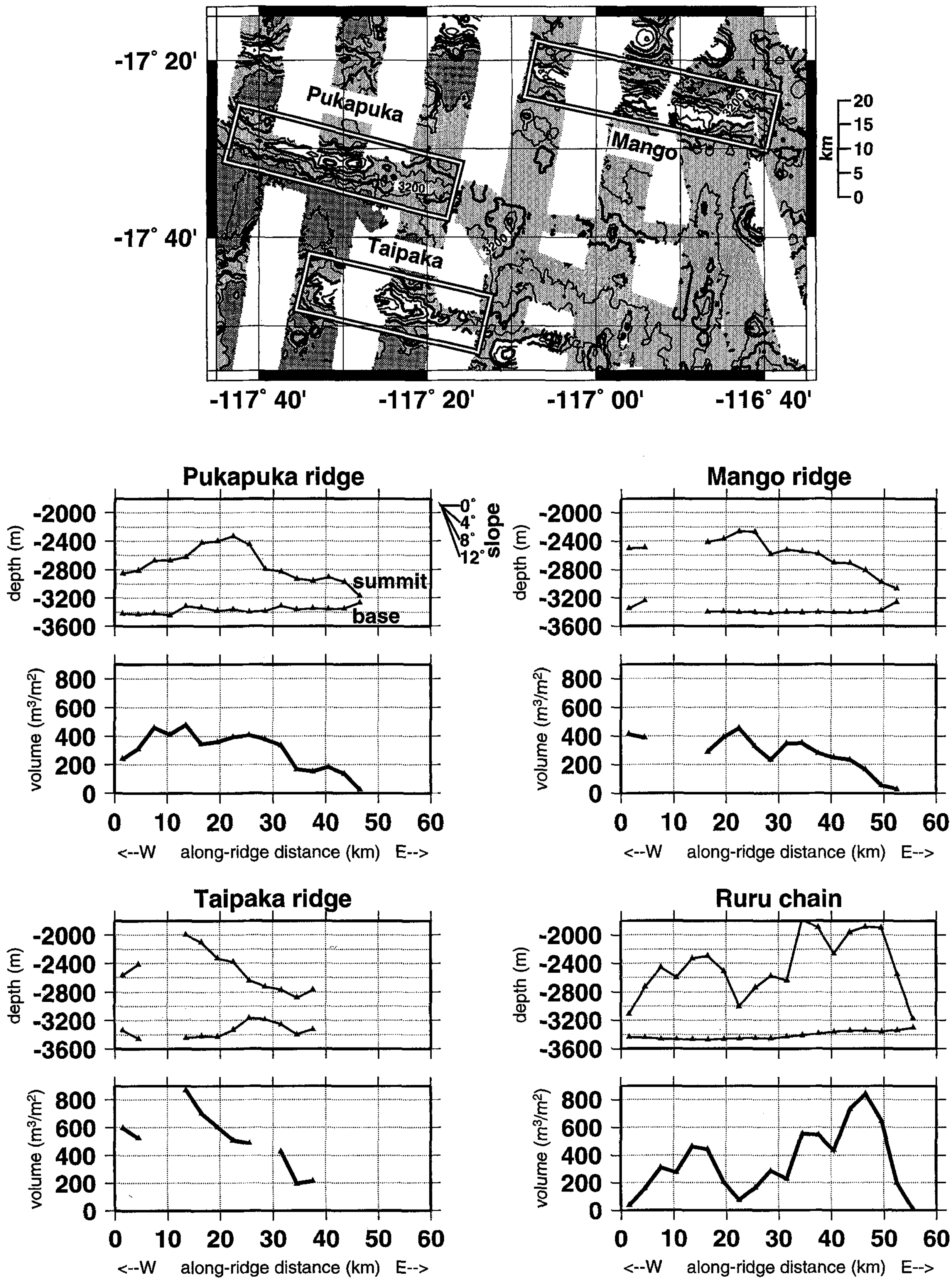

-17° 20'
-17° 40'
-117° 40'
-117° 20'
-117° 00'
-116° 40'
Pukapuka
Mango
Taipaka
3200
km
20
15
10
5
0
Pukapuka ridge
Mango ridge
Taipaka ridge
Ruru chain
depth (m)
-2000
-2400
-2800
-3200
-3600
summit
base
0°
4°
8°
12°
slope
volume (m³/m²)
800
600
400
200
0
0 10 20 30 40 50 60
<--W along-ridge distance (km) E-->

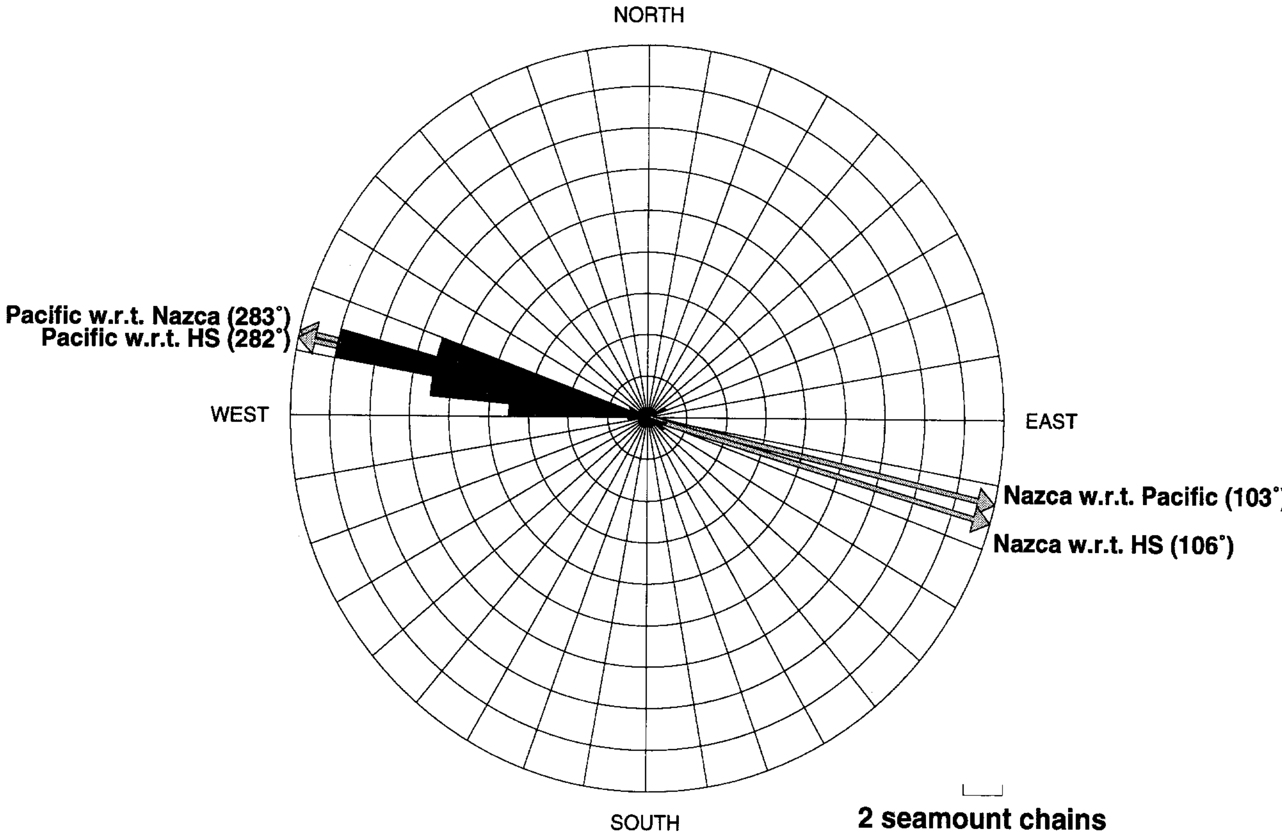

Fig. 8. Rose diagram of the orientations of the SEPR seamount chains from Table 2. The absolute and relative plate motion vectors are nearly collinear on both plates.

towards the axis. The Providence chain probably is also split near 16° 30' S, 113° 50' W. Other chains west of 116° 30' W, where sidescan and bathymetry coverage is only 50%-complete, may exhibit similar behavior. These observations suggest that a single point-source which is stationary and maintains a vertical ascent path does not exist throughout the lifetime of these complicated chains. The complex morphology of the Hotu Matua chains is unlike that of any other seamounts in this area, Figure 4e. These clusters, which contain the largest edifices surveyed, are flanked by volcanic ridges and numerous, sometimes large, volcanoes off the main centers of volcanism.

← Fig. 7. Examples of volcanic ridges (top) in the westernmost portion of the survey. Smaller panels display the along-ridge summit and basal depths and the along-ridge edifice volume for three of the ridges, indicated by the boxes in the map. The along-ridge volume is normalized to the area of coverage for each along-ridge distance bin. For comparison, the depth and volume profiles of the Ruru chain (Figure 4b), composed of overlapping edifices, are plotted in the lower right.

Seamount Production and Axial Morphology of the SEPR

Scheirer and Macdonald (1995) document a correlation between greater seamount abundance and signs of enhanced ridge magmatism at the fast-spreading NEPR. This area of the SEPR is devoid of any discontinuity larger than 5 km in offset, and the variations in axial depth and cross-sectional area are small relative to those of the NEPR (Scheirer and Macdonald, 1993). Nonetheless, the largest-offset OSC at 15° 55' S and its scars off-axis (Cormier *et al.*, this issue) are nearly devoid of seamounts. This section of the ridge crest is also associated with the disappearance of the otherwise nearly continuous and shallow axial magma chamber reflector (Detrick *et al.*, 1993). It is ambiguous, however, whether the lack of seamounts near the OSC is a direct consequence of the discontinuity's presence as the OSC is situated in the broad, relatively seamount-free half of the study area.

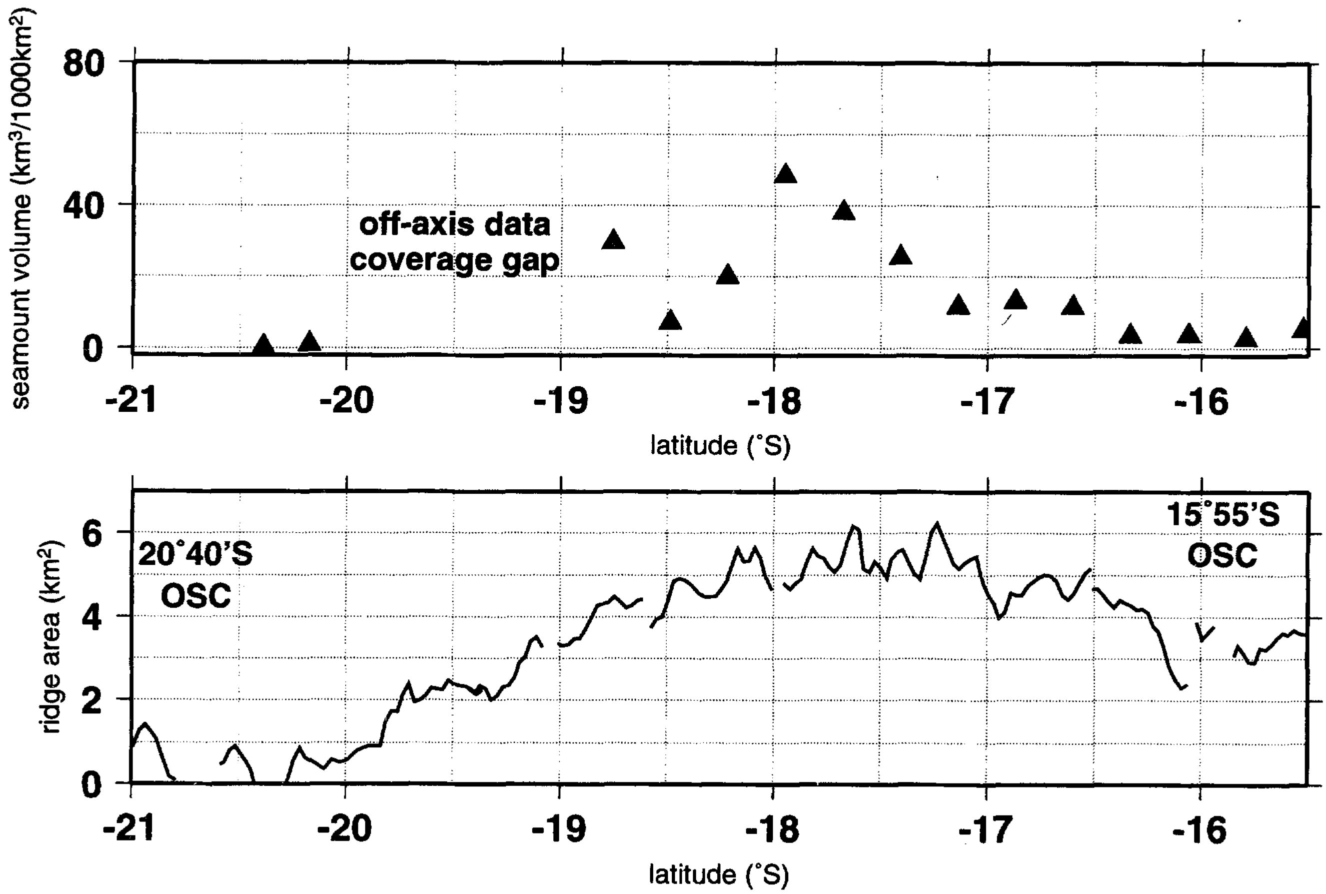

Fig. 9. Variation in the volume of seamount edifices vs. latitude. a) Seamount volumes represent the total volume of edifices within 50 km-wide corridors oriented perpendicular to the axis, on crust aged $\leq$0.8 Ma, normalized to the area of coverage of seafloor. b) Variation in the cross-sectional area of the ridge axis (Scheirer and Macdonald, 1993).

A larger discontinuity (> 8 km offset) existed in the past (>~ 0.8 Ma), and its scars are presently at a latitude of ~ 17° S (Cormier *et al.*, this issue). These scars do not seem to correlate with either a greater or lesser abundance of seamounts. Further comparisons of seamounts with discontinuity scars are difficult because of the asymmetry in the swath coverage about the SEPR and the concealment by seamount edifices and flows of the tectonic lineaments inherited from near the axis.

Figure 9 displays the variation in volume of all seamount edifices in 50 km wide, ridge-perpendicular corridors which are spaced every 30 km along-axis. In this plot, we include some data north of the 20° 40' S OSC from a survey centered on 20° S. We consider only those seamount edifices situated on crust younger than 0.8 Ma, as seamounts on older crust may have formed in the vicinity of an axial ridge which had different properties from those of the current axis. At long wavelengths, there appears to be a fairly good, direct relationship between cumulative seamount edifice volume and cross-sectional area. In particular, the cumulative seamount volume near the 15° 55' S and 20° 40' S OSC's is diminished.

A similar, but noisy, direct relationship between off-axis seamount edifice volume and ridge cross-sectional area was noted in Scheirer and Macdonald (1995), which led to the assumption of some causal connection between inflated ridges and the production of adjacent seamounts. The SEPR relationships are consistent with the notion that along-axis variations (due to temperature, mantle composition?) in the melt feeding the spreading center may extend off-axis and be expressed as variations in seamount production.

Recent Seamount Volcanism and Evidence for Mass-Wasting

Highly reflective areas observed in sidescan data near the SEPR delimit young, relatively unsedimented seafloor. The axis of the SEPR is very reflective, and the seafloor decreases in reflectivity with distance from the axis as sedimentation smoothes the small-scale surficial roughness and diminishes the acoustic impedance contrast of the seafloor interface. For this portion of the SEPR imaged at ~ 12 kHz (common to the swath mapping systems), a zone extending to ~ 7 km on both sides of the axis is very reflective (Figure 4a). Between 7–15 km (~ 90,000–200,000 years), the seafloor decreases rapidly in reflectivity; beyond this zone, the only common sidescan events arise from abyssal scarps and seamounts. We interpret the high backscatter seafloor in the flat areas surrounding seamounts to be associated with lava flows younger than ~ 200,000 years. Some observed flows have very high reflectivity and are probably younger than 50,000 years, but more direct means of dating are necessary to refine these estimates.

An alternative explanation of the source of some of the highly reflective seafloor arises from fields of manganese nodules (Winterer, personal comm.), as was inferred along the Pukapuka Ridge west of our survey. If this is the case, some local conditions around seamounts might be conducive to manganese nodule formation. We note, however, that all of the reflective areas sampled in our study area during Gloria leg 8 (Sinton *et al.*, 1993) returned fresh basalt samples.

Numerous patches of high reflectivity surround seamounts scattered throughout the study area, Figure 10, on crust aged < 1 Ma to over 6 Ma (> 450 km from the axis). Many of these areas were dredged during Gloria leg 8 (Sinton *et al.*, 1993) six months after our Melville legs; these dredges recovered glassy basalt samples, many of which would have looked in-place had they been dredged from the ridge axis (John Sinton, personal comm.).

Some high reflectivity flows completely surround the seamounts while others exist only to one side. Their distal edges often have irregular outlines (Figures 4a, 4c, 4e, 4f), analogous to those of subareal flows. Sometimes the flows are bounded by abyssal scarps or are restricted to the moat depressions around large edifices. The general lack of abyssal lineaments surrounding seamounts is interpreted to indicate that lava flows and mass-wasted material is thick enough to cover these abyssal scarps (Shen *et al.*, 1993), which locally range in height from ~ 40–100 m. The sedimentation rates in this remote part of the Pacific are small, with estimates ranging between < 1 and 26 m/Myr (Dekov and Kupstov, 1990; Dekov and Kuptsov, 1992; Lyle *et al.*, 1987; Marchig *et al.*, 1986), generally falling between 3 and 6 m/Myr. In the Gloria cruise 3.5 kHz echosounder data, we regularly observed sediment thicknesses less than ~ 0.05 sec (~ 50 m thick, assuming a sediment velocity of 2 km/sec) in the westernmost portion of the survey, and insignificant thicknesses along the entire Eastern MELT corridor. Thus, over the entire study area, the sediment thickness is less than ~ 150 m (probably less than 50 m) and is insignificant compared to the height of volcanic edifices included in this study.

A number of seamount chains exhibit fresh lava flows at their near-axis ends (such as Cloud, Toroko, and Providence) while others exhibit fresh flows scattered along their entire length (Beraiti, Hurihuri, Carberry, Teka), Figure 10. The two largest regions of fresh flows surround the Hotu Matua and Apitoka chains, in the western corners of the survey, where young volcanism covers areas of 3000–4000 km^2 on crust aged 5.0–6.5 Ma. The extensive flows imply that the eruption rate and/or magma viscosity is such that the lava can flow far (> 20 km) from the steep edifice slopes. The existence of fresh flows far from the SEPR contrasts with the near-absence of acoustically reflective flows surrounding seamounts beyond ~ 20–30 km from the axis of the NEPR (Scheirer and Macdonald, 1995). Several edifices on older crust which are associated with fresh flows at their bases do not have reflective summit regions, suggesting that some late-stage volcanism may emanate from the flank or the base of a seamount. The sea surface-based sidescan data do not provide a clear picture of the vents feeding these reflective flows.

Another alternative explanation for the reflective seafloor surrounding some of the Rano Rahi Seamounts is the presence of landslides from the flanks of these edifices. Recent comprehensive studies around the Hawaiian Ridge (Moore *et al.*, 1994) have recognized and classified mass-wasting features which produce distinctive patterns in sidescan sonar images of these volcanoes and the surrounding seafloor. Slumps produce distinctive tensional scarps at their heads and compressional bulges and steep toe-fronts distally; debris avalanches produce well-defined amphitheaters at their heads and lobate, hummock-dominated toes. None of these morphologic features is obviously associated with the reflective seafloor patches near the Rano Rahi seamounts, which are generally uniformly bright and have little measurable topographic variation.

Although we do not favor the possibility that the off-axis reflective seafloor surrounding some of the Rano Rahi seamounts is due to landslides, there is ample evidence that various degrees of mass-wasting have been important in the development of some of these volcanoes. The southern flank of the seamount centered at 17° 05' S 117° 13' W appears to be a large-

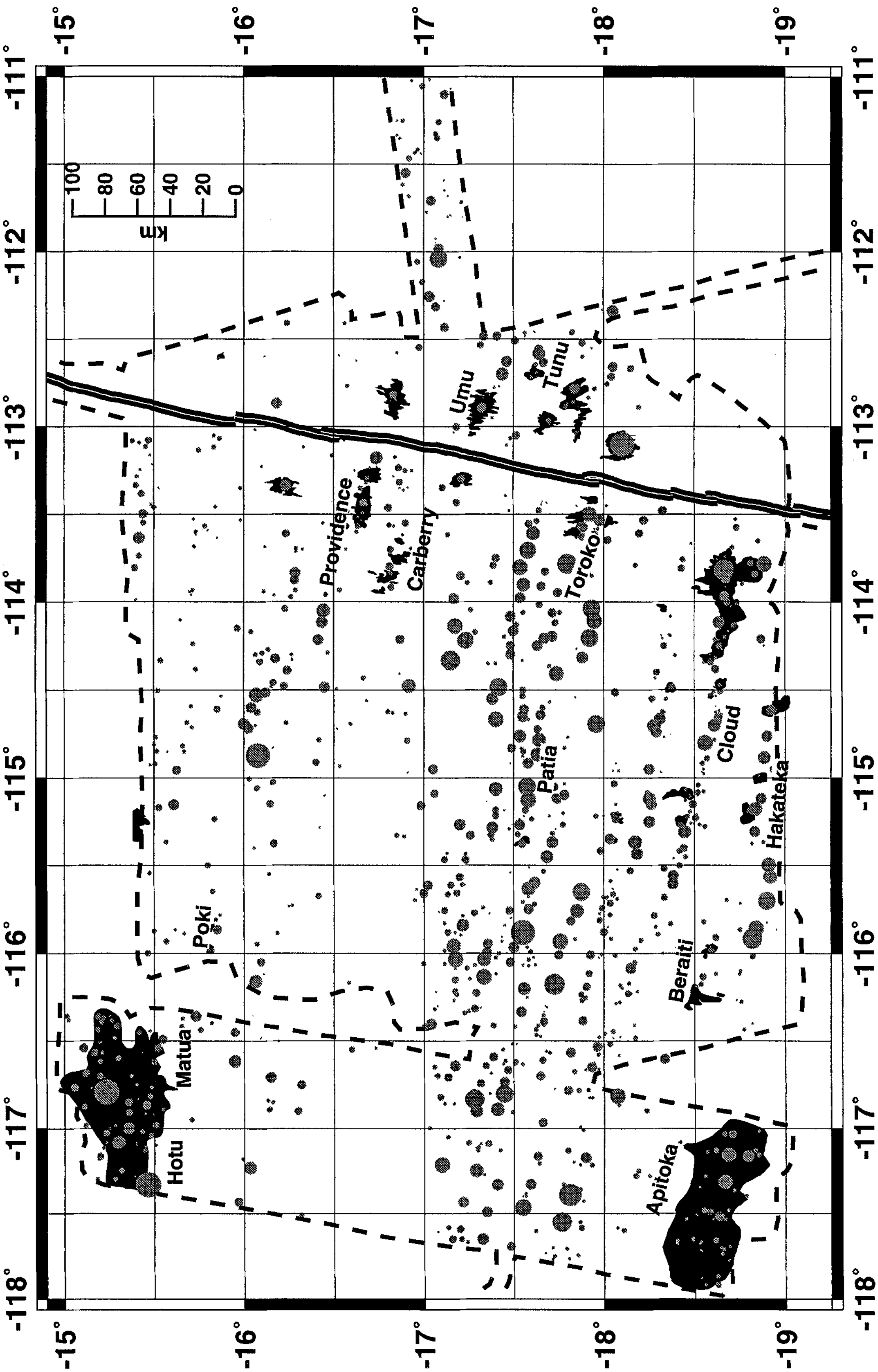

Fig. 10. Acoustically reflective seafloor, black-fill, which is adjacent to off-axis seamounts. Names are provided for those chains associated with inferred fresh lava flows.

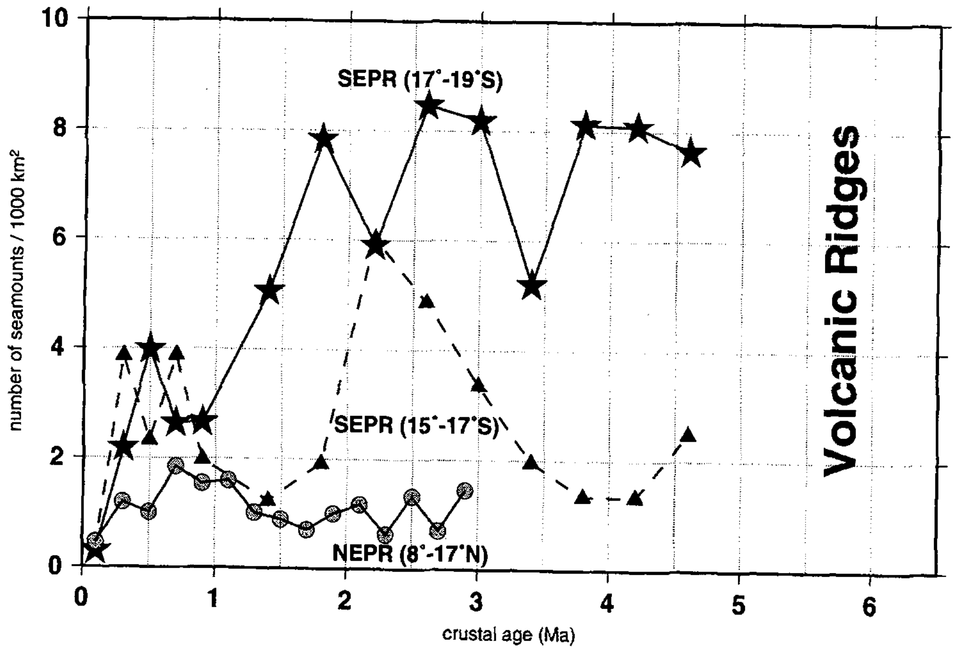

Fig. 11. Abundance of seamounts taller than 200 m versus crustal age for the northern and southern halves of the study area and for the NEPR. The time-span represented by each point for the SEPR curves increases from 0.2 Myr to 0.4 Myr where the bathymetry coverage decreases significantly at 1 Ma.

scale collapse from a prior conical form; the toe of this inferred landslide runs partially up the slope of a neighboring volcanic ridge. Other departures from circular symmetry and indentations of seamount flanks may be the result of mass-wasting, and it has been recognized that the volume of material filling in the moats surrounding the larger edifices and obscuring the ancestral abyssal hill fabric may be due to both mass-wasted material and lava flows (Shen *et al.*, 1993). As inferred by Moore *et al.* (1994), the primary period of movement of the landslides seen today occurs at the end of vigorous, shield-building volcanic activity of the Hawaiian Ridge. Similarly, we expect that mass-wasting of the Rano Rahi volcanoes might also occur during and immediately following their major growth periods, as flank slopes and seismicity are maxima.

Seamount Abundance Versus Distance from the Axis

Along the entire surveyed EPR between the Rivera Transform (18° N) to the Easter Microplate (23° S), there are no seamounts $\geq$200 m high within 5 km of the ridge axis (Edwards *et al.*, 1991; Scheirer and Macdonald, 1995). However, many seamounts are present, including very large ones, within ~40 km (~0.5 Ma) of the axis in the SEPR (Figure 3a) and NEPR study areas. Figure 11 displays the observed number of seamounts per 1000 km^2 of bathymetry coverage versus crustal age from three well-surveyed areas: the SEPR 17°–19° S, the SEPR 15°–17° S, and the NEPR 8°–17° N. In all three areas, the seamount abundance increases rapidly from near-zero in the youngest 0.2 Myr age bin to much greater values in the next two bins. Beyond ~0.5 Ma, the rate of increase in seamount abundance slows or levels off altogether. Whereas the NEPR dataset achieves a long-term abundance between 1 and 2 smts/1000 km^2, the SEPR abundances are greater. The 15°–17° S curve fluctuates greatly, mostly due to the effects of the relatively few seamount chains (especially at ~2 Ma where the Santa chain dominates), but it is at a higher level than that of the NEPR. The 17°–19° S curve increases more or less steadily to about 2.5 Ma, at levels several times greater than the other two curves. Thus, in the southern half of the study area, greater numbers of seamounts appear to form in a much broader zone than elsewhere.

To address the growth behavior of these seamounts, we calculate the variation in seamount edifice volume with age of the crust by isolating the seamounts from gridded bathymetry using the median filtering technique of Shen *et al.* (1993). This method identifies as belonging to seamounts those portions of seafloor which are significantly shallower than the median depth in a specified region of surrounding seafloor. We removed the seamount edifices using a box 30 km long and 2.4 km wide, aligned parallel to the ridge axis; these dimensions are slightly larger than those of

Shen *et al.* (1993) to allow for larger seamount edifices and less complete bathymetric coverage. An example of the output of this analysis is displayed in Figure 12, showing the isolated seamounts from a southern portion of the survey.

The total volume of seamount edifices, based on the gridded removal technique of Shen *et al.* (1993), is 9100 km^3. Assuming an average crustal thickness of 6 km, this volume constitutes ~ 0.08% of the volume of the surveyed crust in this area. The volume of lava flows and mass-wasted material surrounding the seamount edifices is probably similar to the edifice volume, as described by Shen *et al.* (1993) from a subset of these seamounts near the axis. This analysis becomes more difficult at further distances from the axis, however, because more scarps are covered by sediments, and it becomes difficult to delineate the areas around seamounts which are covered with material derived from the seamounts. The volumes of individual seamounts range from < 0.02 km^3 to 300 km^3.

The volume of seamount edifices versus crustal age for the NEPR, SEPR 15°–17° S, and SEPR 17°–19° S areas are displayed in Figure 13. The volume of the NEPR and SEPR 15°–17° S seamounts are dominated by the effects of a few large seamount chains; for the SEPR 15°–17° S, the increased volume between 2–3 Ma is primarily due to the Santa chain. In these two areas, the volume increases rapidly on crust aged < 0.5 Ma; beyond this age, the volume of seamounts fluctuates mostly between 10 and 50 $km^3/1000\ km^2$. Conversely, the volume of the SEPR 17–19° S seamounts increases more or less continuously out to ~ 3.5 Ma, reaching levels of 100–150 $km^3/1000\ km^2$, mostly due to the large seamount chains which become more abundant with greater distance from the axis. The extent to which fluctuations in seamount abundance (Figure 11) or volume (Figure 13) reflect temporal variations in growth rates in a constant zone of formation versus temporal variations in the locations and intensity of seamount formation is unknown. Given the rapid increase of these measures between the ridge axis and ~ 1 Ma, however, we do favor a model where the bulk of the volcanic activity occurs in that age range.

The rate of growth of individual volcanic edifices is an important, but not very well-understood property of these seamounts. We can estimate the minimum edifice growth rate by dividing the volume of large seamounts which lie on young crust by the age of the crust. The four largest seamounts on crust younger than 0.5 Ma have minimum growth rates between 25 and 250 km^3/Myr. Considering that these seamounts do not seem to have formed in the innermost 5 km about the axis, these minimum rates increase by 10–15%. An eruption rate of 100 km^3/Myr is at the low end of the range of rates for continental volcanoes compiled by Trial and Spera (1990), and it is two orders of magnitude less than the average hot spot output along the Hawaiian-Emperor chain (Clague and Dalrymple, 1989). We emphasize that the growth rates calculated for these large, near-axis seamounts are minima; actual rates could be significantly greater. Also, we do not have evidence for the rates of volcanic growth of small edifices or of those further from the axis.

Seamount Magnetization Analysis

The magnetization of seamounts relative to that of the crust they lie upon provides a crude technique to date the formation of the seamount edifices. Barr (1974) observed an only-slight disruption of the magnetic isochrons near seamounts along the Juan de Fuca Ridge and inferred their construction to be very near the axis. Likewise, Scheirer and Macdonald (1995) note that the vast majority of the NEPR seamounts which are oppositely magnetized from their underlying crust fall within 25 km of the nearest younger seafloor having like magnetization. Hence, these seamounts may have formed within 25 km of the ridge axis. Although this dating method is non-unique (a seamount of a particular magnetization may have formed during *any* time of like magnetization younger than the age of the underlying crust), this timing control applied to the Rano Rahi seamounts is useful in a number of ways.

The nearly north-south orientation of the tracklines, approximately perpendicular to the orientation of the seamount chains and parallel to the magnetic anomaly stripes, is favorable to sample the dipolar magnetic anomalies from the seamounts and volcanic ridges. These anomalies, which may be quite large (> 200 nT), arise primarily from the shallow seamount topography; seamounts with dipole anomalies positive to the north are primarily normally magnetized, and seamounts with negative anomalies to the north are primarily reversely magnetized (Figure 14). We evaluated the anomalies associated with the 411 seamounts taller than 300 m (the minimum size which can produce a discernible anomaly at the sea surface). Our results are plotted in Figure 15 and summarized in Table III. Of all of the ≥ 300 m tall seamounts, 303 edifices do not have discernible dipolar anomalies, as many are too small, are not crossed by ship tracks, or are adjacent to larger seamounts and/or magnetic reversal boundaries. However, 28 of the seamounts without discernible magnetization do have adequate coverage and are large enough to produce significant anomalies; some of these

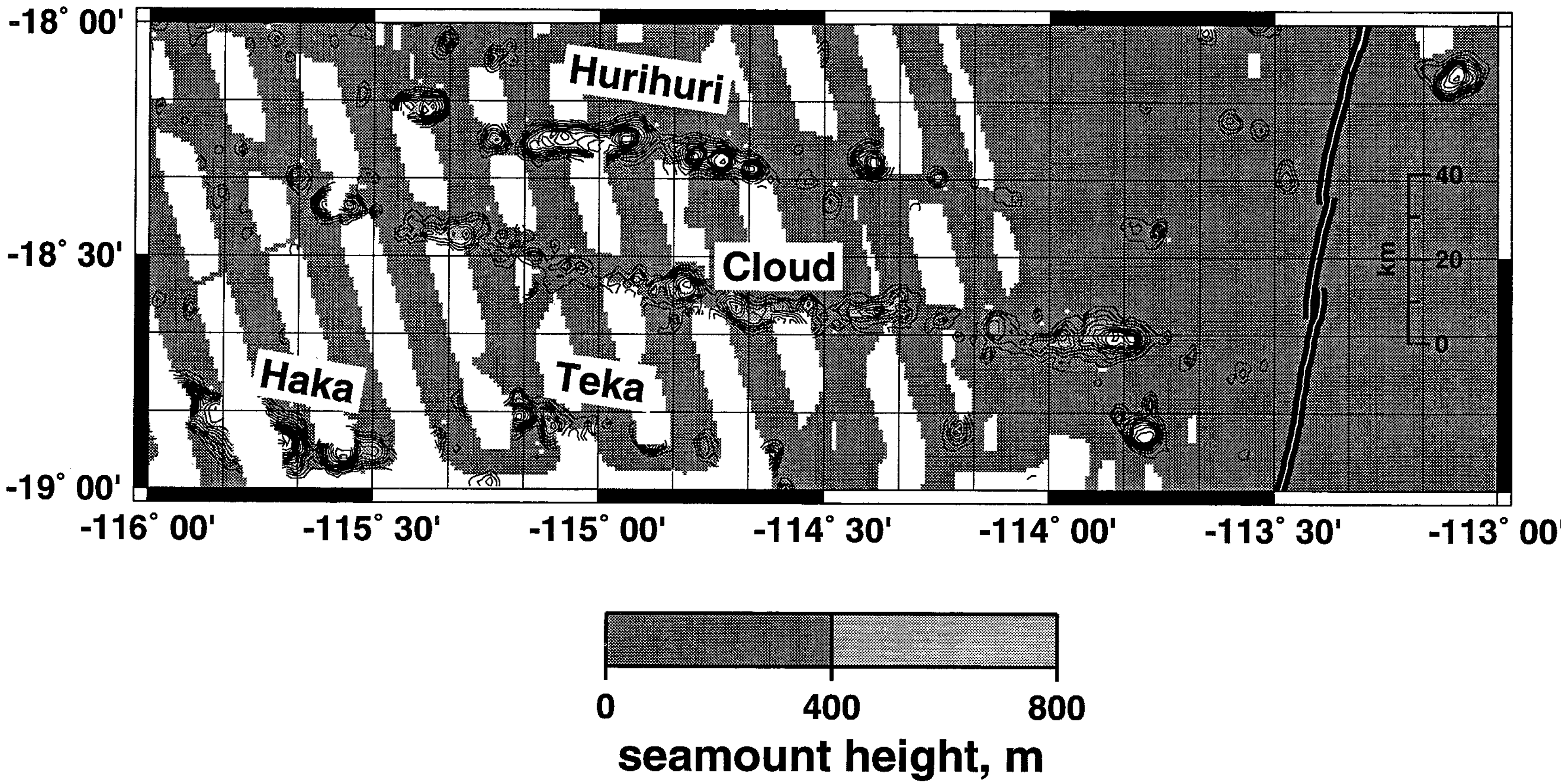

Fig. 12. Results of median-filter seamount removal for a southern portion of the survey area. Seamounts are contoured every 100 m.

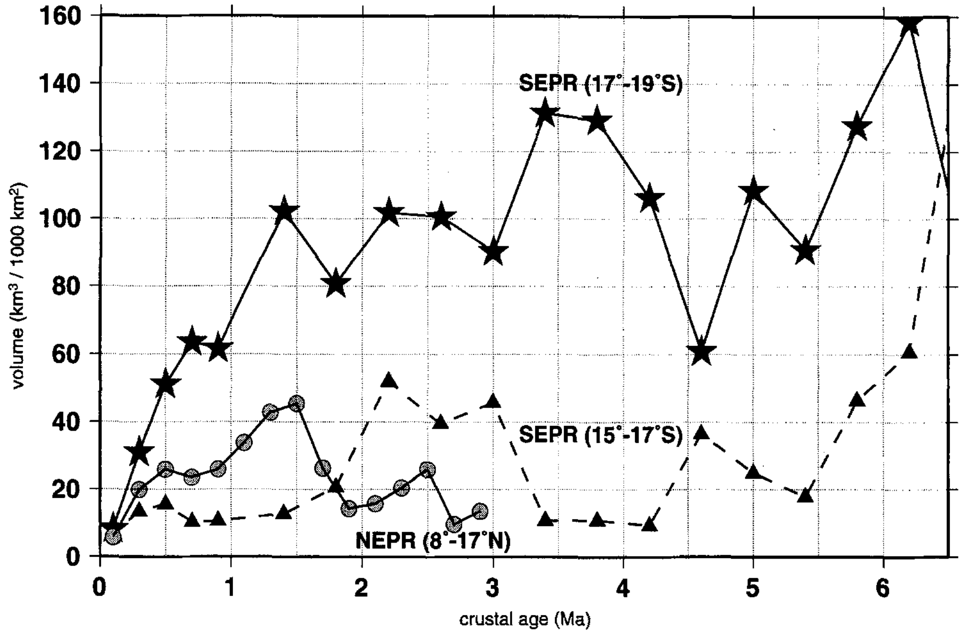

Fig. 13. The volume of seamount edifices vs. crustal age. The time-span represented by each point for the SEPR curves increases from 0.2 Myr to 0.4 Myr where the bathymetry coverage decreases significantly at 1 Ma.

seamounts have virtually no associated magnetic anomaly, and others have non-dipolar anomalies. This indicates either that the magnetization of the seamount material is low, or perhaps that the seamount did not grow during a time interval of uniform geomagnetic field.

Of the 108 seamounts with discernible magnetization, 71 have well-determined magnetizations (crosses in Figure 15). Most of the long seamount chains contain seamounts having different magnetizations, indicating their time-transgressive origin. For example, the Cloud chain is composed of several normally magnetized edifices to the east, then reversed edifices, and probably another normal and reversed pair further to the west. Hurihuri has a similar history. The volcanic ridge Apitoka, in the southwest corner of the survey, clearly has sections of both magnetizations; hence, it did not form synchronously along its entire length. With 20 km line-spacing and variably sized seamounts along any given chain, it is difficult to associate the reversal sequence of a seamount chain to that of the seafloor stripes, especially where the stripe pattern is characterized by rapid reversals, e.g. during chrons 2A and 3.

Another observation is that, in a number of cases, clearly reversed seamounts are surrounded by highly reflective seafloor, reflectivity which is inferred to arise from fresh, unsedimented lava flows. As noted above, if the sedimentation rate near the seamounts is similar to that at the ridge axis, then highly reflective seafloor is at most 200,000 years old (and probably less than 100,000 years old). Since the most recent time of reversed polarity was nearly 800,000 years ago, the magnetically important bulk of these edifices seems to have formed much earlier than the reflective lava flows. The western half of the volcanic ridge Apitoka is clearly composed of reversely magnetized rocks, even though the entire ridge is surrounded by reflective seafloor which extends 10–20 km from its base (Figure 15). Likewise, a number of edifices in Hotu Matua, Figure 14, produce clear reversed dipoles in association with reflective seafloor. Also, a large, isolated edifice near 18° S, 114° 40' W is clearly reversed and appears to be surrounded by flat seafloor having high reflectivity. The simplest explanation for these observations is a two-stage eruption history: first the major portion of the edifice is formed during a reversed time period (imparting its magnetic signature), then the areally extensive lava flows form (within the past 200,000 years). These latter flows might not create a measurable magnetic anomaly at the seafloor because they have low magnetization, because they are thin, or, most likely, because they lack relief. Such a multi-stage growth scenario has important geologic implications, such as the possible inheritance of melt pathways near existing edifices by later-formed magmas. These implications

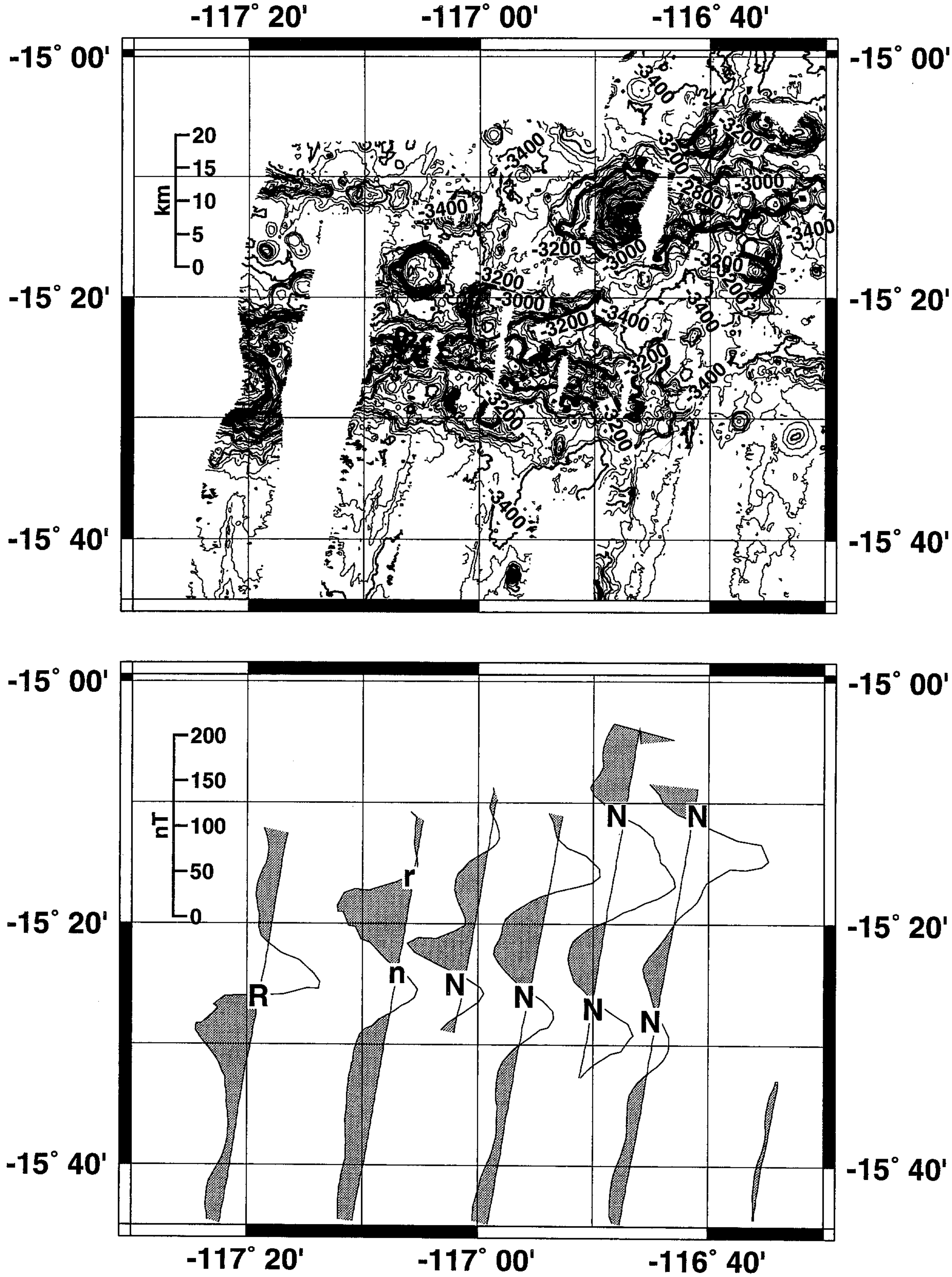

Fig. 14. Bathymetry (top) and magnetic anomalies (bottom) of the Hotu Matua area, along with inferred seamount magnetizations. N = normally magnetized, n = probably normally magnetized, R = reversely magnetized, r = probably reversely magnetized.

TABLE III
Seamount magnetization summary

Out of 411 seamounts ≥300 m tall:
303 seamounts do not have discernible magnetization
120 of these do not have adequate track coverage
28 of these are large and have adequate coverage but no clear dipolar anomaly
108 seamounts have discernible magnetization
68 N seamounts
40 R seamounts
Out of 108 seamounts with discernible magnetization:
45 seamounts are magnetized oppositely from the crust they lie on
34 N seamounts on R crust**
11 R seamounts on N crust
** 6 of these normally magnetized seamounts on reversed crust lie ≥25 km from the nearest younger isochron; hence, they formed, in bulk, at least 25 km from the ridge axis

N = normally magnetized; R = reversely magnetized.

may be better characterized by geochemical and geochronologic analysis of the volcanic products.

There are six seamounts, of the 45 which are oppositely magnetized from the crust they lie on, which lie beyond 25 km from the nearest younger time of like magnetization. Four of these examples, illustrated in Figure 16, are normally magnetized seamounts on the wide, reversed intervals between anomalies 2A and 3 and between anomalies 3 and 3A. Their setting indicates that most of their edifices formed at least 28 to 50 km from the ridge axis, a zone much wider than that inferred for the NEPR seamounts (Edwards *et al.*, 1991; Scheirer and Macdonald, 1995). This wider zone is consistent, however, with the wider zone of growth of the SEPR seamounts, described in the previous section.

Finally, we note that within ~ 120 km of the axis (out to ~ 114° 30' W, Figure 16) and where tracklines are spaced every 10 km, the seamount magnetizations cluster into three groups. From east to west, there are a number of well-determined normally magnetized seamounts, then some ambiguous ones, then well-determined reversed seamounts. The first group most likely formed during the current Brunhes epoch and the latter group during the long, mostly reversed interval between the Jaramillo (1a) and 2a anomalies. The ambiguous seamounts probably formed during the two, relatively short intervals between the old sides of both the Brunhes and the Jaramillo anomalies.

The Formation of Near-Axis Seamounts

To produce a seamount, some amount of mantle upwelling must generate a batch of melt which is large and mobile enough to penetrate the overlying lithosphere before it freezes entirely. To produce a seamount near a spreading center, these batches of melt must escape the processes which concentrate MORB melt in a very narrow neovolcanic zone about the axis.

A number of models are considered for the origin of near-axis seamounts; these are sketched in Figure 17 and include:

1. Preferential, early melting of small embedded fertile mantle heterogeneities in the upwelling beneath a spreading center (Davis and Karsten, 1986; Wilson, 1992), Figure 17a.
2. "Miniplumes" due to thermal and/or chemical instabilities in a low-viscosity layer somewhere in the mantle (Barone and Ryan, 1990; Desonie and Duncan, 1990; Shen *et al.*, 1993; Shen *et al.*, 1995), Figure 17a.
3. Mantle upwelling associated with ridge-perpendicular convection which produces the extensive gravity lineaments (Scheirer *et al.*, 1993; Shen *et al.*, 1993), Figure 17b.
4. Lithospheric stretching or "boudinage" associated with the formation of the gravity lineaments (Dunbar and Sandwell, 1988; Sandwell and Dunbar, 1988; Winterer and Sandwell, 1987), Figure 17c.
5. Three-dimensional, time-dependent convection in the mantle (Shen *et al.*, 1993).
6. Some other cause related to unusual lithospheric and/or asthenospheric properties beneath the Pacific seafloor, Figure 17d.

As possible causes for the SEPR seamounts, these models are not mutually exclusive. They rely to varying degrees on the nature of mantle heterogeneity, modes of mantle upwelling, and the ease of penetration of the lithosphere. The latter two models are not specific nor do they provide testable predictions for the existing dataset.

We evaluate these models by addressing a number of fundamental questions, which largely relate to seamount chains:

a) To what extent are the seamounts formed by processes involving point-sources or line-sources?
b) How does the flux of material from the seamount source vary through time along an individual chain?
c) How are nearby seamounts and seamount chains related to one another?
d) How does the distribution of seamounts relate to other geological phenomena such as proximity to the ridge axis, discontinuity scars, asymmetric subsidence, and the gravity lineaments?

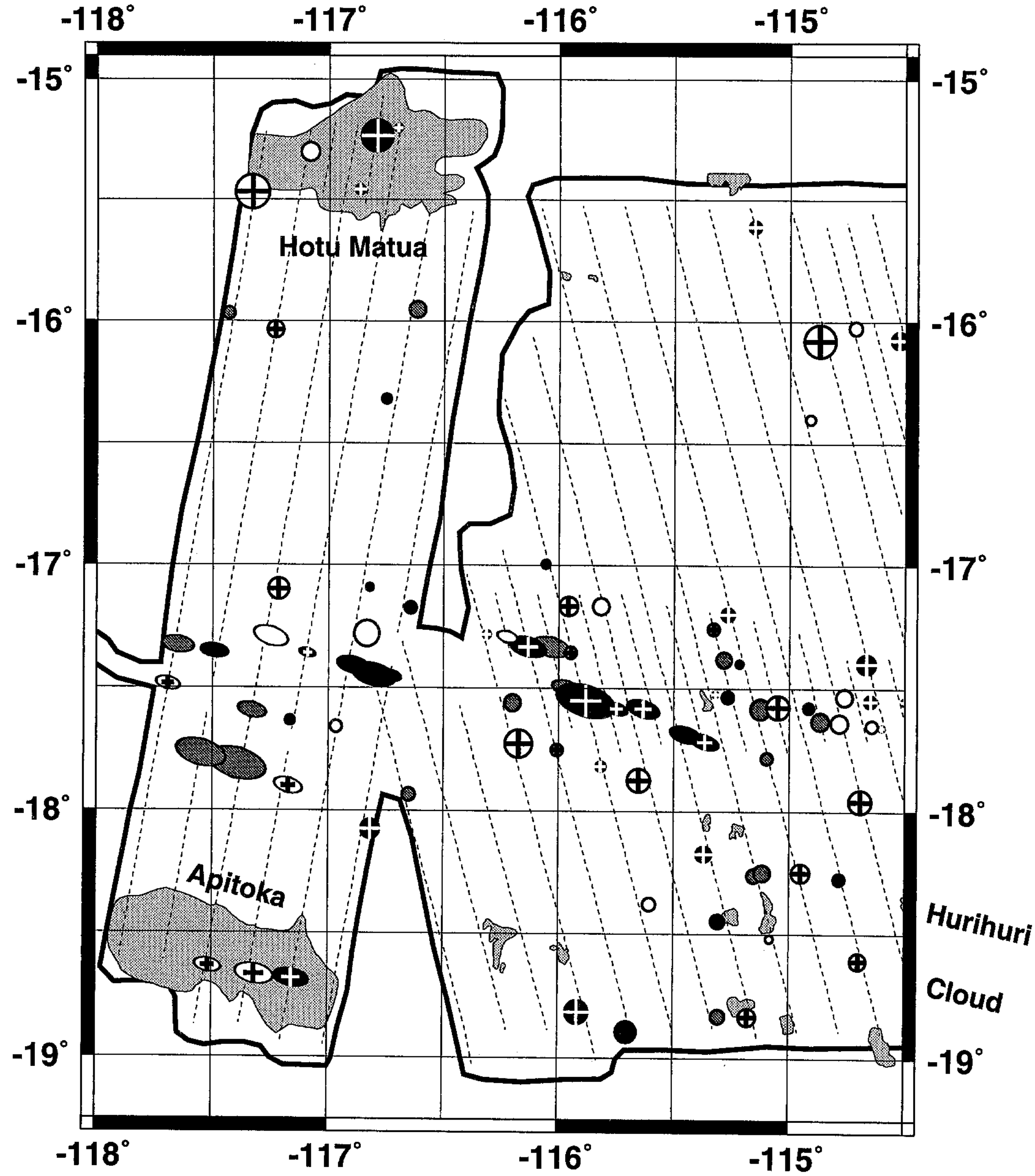

Fig. 15a.

POINT-SOURCE VS. LINE-SOURCE

In this discussion, we use the term "source" of a seamount to be that mantle region where the magmas form which ultimately lead to the construction of a seamount. If, like a typical hotspot chain, the source of magma is small (in plan view) with respect to the length of a seamount chain, then that source may be considered as a point-source. With a point-source, seamount chains would form asynchronously with the oldest volcanoes towards the direction of plate motion. Alternatively, if the source of magmas is aligned horizontally beneath a chain, then the seamount chain could have formed synchronously. The relationships between the mantle melting region, melt ascent and accumulation in the lithospheric mantle and crust, and ultimately its eruption on the seafloor are poorly understood; nonetheless, it is useful to consider these end-member models of the mantle source and their possible manifestations as volcanism on the seafloor.

A number of chains, particularly those near the axis such as Toroko and Cloud, tend to have more reflective flows towards their near-axis ends, Figure 10, often surrounding several of the nearest-axis edifices. Sea-

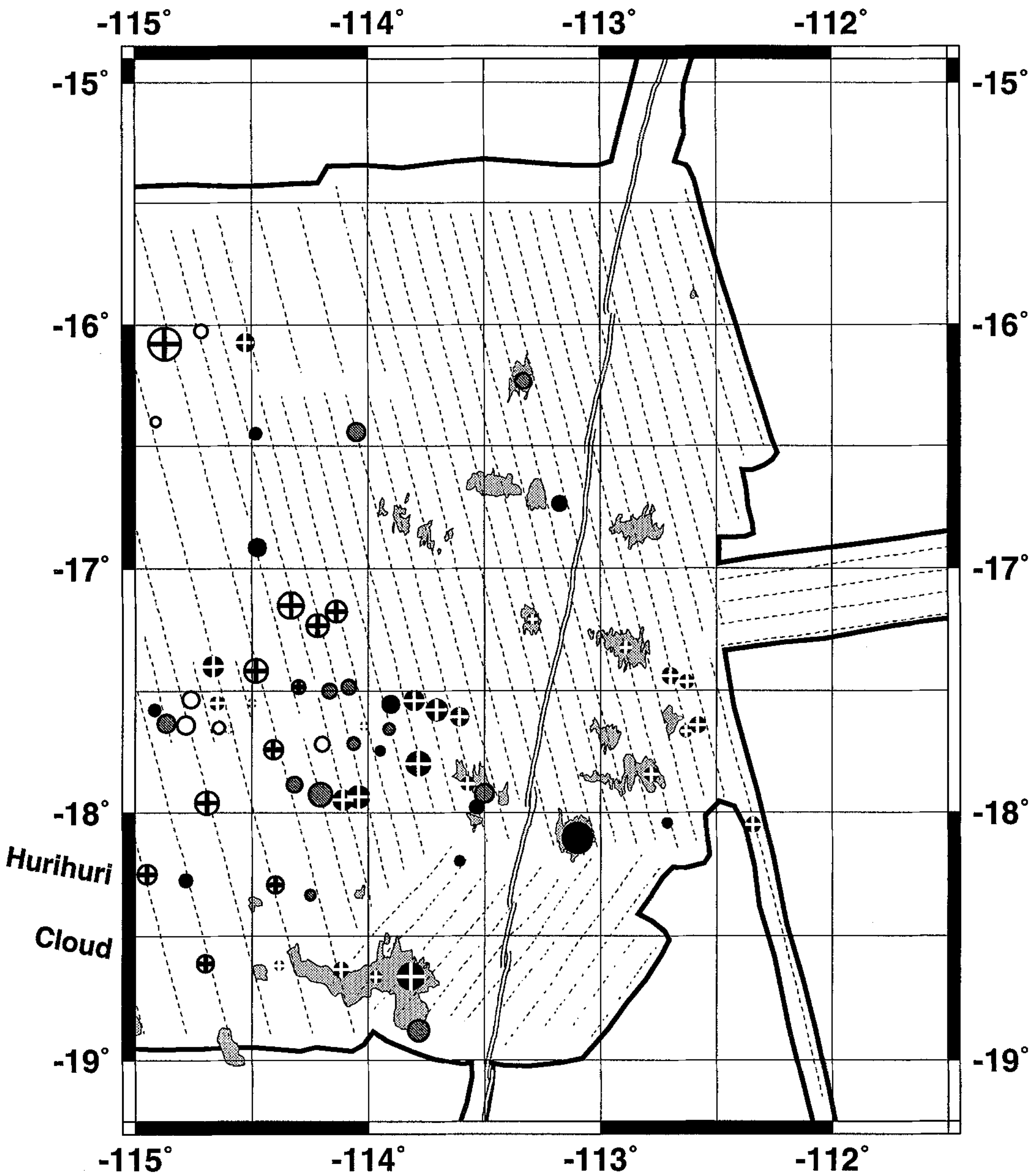

Fig. 15b.

Fig. 15. Seamount magnetization results. Normally magnetized seamounts are filled with black; reversely magnetized seamounts are white. A cross indicates that the seamount magnetization is well-determined. Seamounts are shaded gray where no dipolar anomaly is observed, even though other seamounts of similar size produce clear anomalies. Seamounts which are too small to produce magnetic anomalies at the sea surface and those with inadequate track control are omitted. Seamounts plotted as ellipses are part of volcanic ridges. Track-line control is shown by dashed lines, and lightly shaded areas indicate reflective seafloor.

mount chains on both flanks of the SEPR display such reflective patterns at distances ranging from ~ 5 km to ~ 70 km from the axis. There are exceptions to this observation, though, as the Carberry and Providence seamounts, which are relatively close to the axis, have reflective flows on portions away from the SEPR.

Beyond the ~ 70 km zone, however, there is no tendency for fresh flows to concentrate at the near-axis ends of seamount chains (Figure 10). The Teka, Beraiti (Figure 4c), Hurihuri, and Patia (Figure 4f) chains have reflective flows either distributed sporadically along the chain or concentrated towards the far-from-axis end.

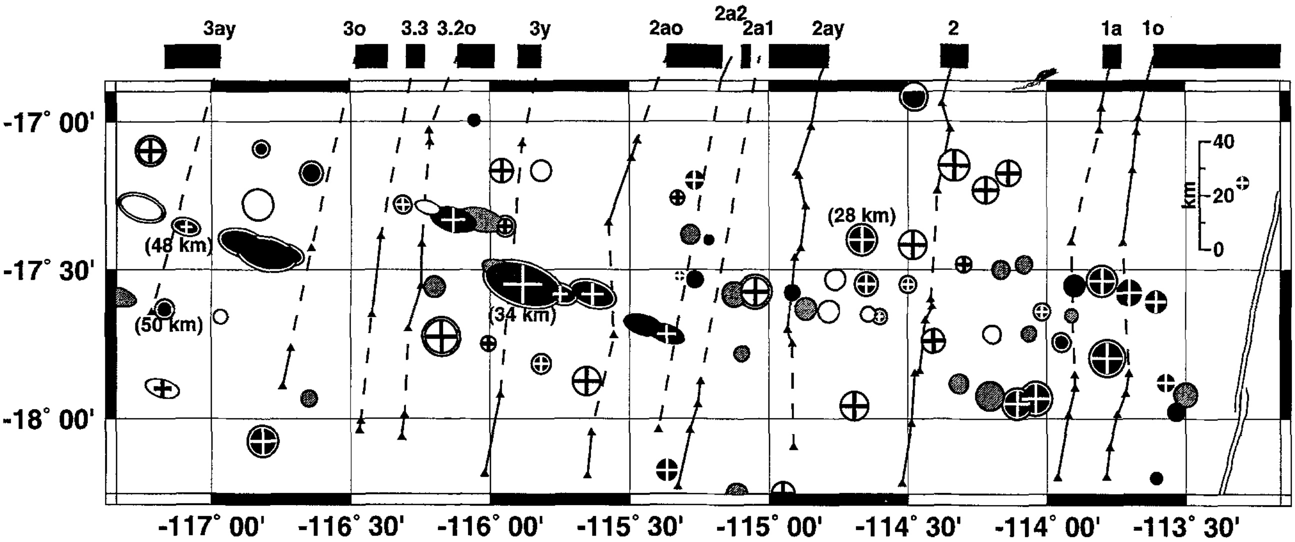

Fig. 16. Expansion of an area of Figure 15, superimposing the magnetic anomaly picks of Wilson (personal comm.). The filled bars above the map indicate the reversal sequence, and anomaly picks are connected by solid lines where close to each other, and by dashed lines elsewhere. Seamounts which are magnetized in the opposite direction from the crust they lie on are surrounded by circles. Four seamounts which are both oppositely magnetized from the crust they lie upon and >25 km from the nearest younger isochron have these distances noted in parentheses.

The two largest off-axis, highly reflective areas completely surround the Apitoka and Hotu Matua (Figure 4e) chains on crust older than 5.5 Ma.

The models of seamount formation involving early-melting heterogeneities and miniplumes (Figure 17a) would both result in the asynchronous formation of seamount chains, predicting younger volcanoes towards the axis. These models might best apply to the recent volcanism on seamounts within 70 km of the axis. To form a long-lived chain, an embedded heterogeneity would need to be elongated along mantle flow-lines, and a miniplume would need to be sustained in one location (or move only slightly with respect to the overriding lithosphere and asthenosphere). The formation of seamounts due to mantle upwelling and lithospheric weakening by ridge-perpendicular convection (Figure 17b) or ridge-parallel stretching (Figure 17c) would favor more lineated seamount sources, so these models might be more applicable to the recent volcanism on seamount chains far from the axis.

We emphasize that the dating resolution available through sidescan reflectivity allows us only to distinguish volcanic activity surrounding seamounts which is either less than or greater than ~ 200,000 years old. Thus, we have only a brief snapshot of volcanic activity across the area that spans more than 6 Myr of spreading.

Another observation which relates to point-source vs. line-source models for the origin of seamounts is the morphology of the Pacific seamount chains. For instance, it seems unlikely that a two-dimensional source beneath the plate would produce distinct and separated volcanic cones at the seafloor unless the plate exerts ultimate control on volcano spacing. Likewise, the production of a volcanic ridge by a point-source is unlikely unless the source supply were very robust and continuous with respect to the speed of the overlying plate or if a shallow plumbing system redistributed melt aligned with the ridge. Hence, the observation that seamount chains are composed of individual volcanoes near the ridge axis and become more ridge-like to the west is broadly consistent with the suggestion of point-sources dominating near the axis with line-sources far from the axis, inferred from seafloor reflectivity, above.

Alternatively, the existence of volcanic ridges in the western part of the survey (to the exclusion of chains composed of individual edifices) may be a function of progressive volcanism which fills between distinct or overlapped edifices. The spatial transition between chains having predominantly distinct edifices to those having overlapped edifices is gradual, occurring between ~ 75 km and 200 km from the axis. The transition from overlapped-edifice chains to volcanic

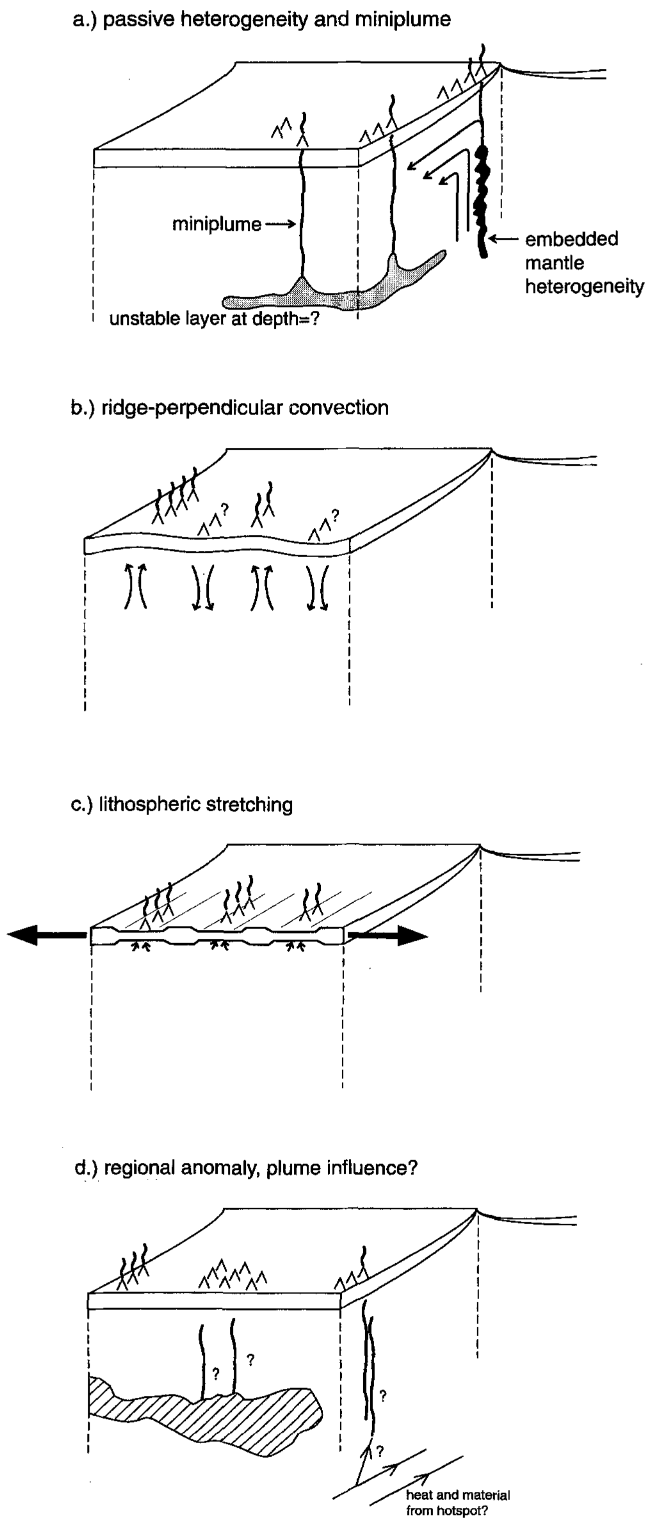

Fig. 17. Cartoons of models proposed for the formation of the seamounts. In (a), the depth of the unstable layer (shaded gray) feeding the miniplumes is thought to be greater than the depth at which asthenosphere has significant horizontal flow.

ridges occurs on crust ~5 Ma; the nature of this transition is unclear, though, due to the loss of 100% HMR1 coverage and nearly complete bathymetry at that age.

Another explanation for the change in morphologic character of the seamount edifices could be that in the past, conditions were more favorable for the production of volcanic ridges near the spreading axis. Through time, the style of seamount volcanism would have changed, resulting in more isolated edifices. Although some of the far off-axis edifices show evidence for recent volcanism, many do not, and the temporal evolution in the style of near-axis volcanism cannot be excluded by our dataset.

Seamount source flux variation

To the extent that seamount chains form asynchronously, variations in the volume of volcanic construction along a given chain should reflect variations in the magma flux from the seamount source. These spatial variations in a chain would occur on time scales equal to the distance along the chain divided by the speed of the overlying plate relative to the seamount source. If the seamount source is stationary with respect to hotspots, then distances along a Pacific seamount chain could be converted to relative ages of eruption by dividing distance by the ~ 100 km/Myr absolute motion rate (since the chains are all closely aligned to the absolute motion vector). Thus, the Cloud chain, at least 240 km long, would represent 2.4 Myr of volcanism, and the typical chain would be active for ~ 0.6 Myr. If the mantle source is somehow tied to the frame of reference of the migrating ridge axis, then the half spreading rate (~ 70 km/Myr for the Pacific flank) would be more accurate for age conversions. If the seamount source in the mantle is moving along with the plate, but at a slower speed, then along-chain distances would represent longer time intervals; conversely, if the source were in flow returning to the axis, then less time would be represented.

Some seamount chains monotonically increase and then decrease in size along their length, such as Anakena and Hikipuku, similar to those near the NEPR (Scheirer and Macdonald, 1995). However, many chains have more complicated fluctuations in volume with several local minima and maxima. The longest seamount chains, Cloud and Hurihuri (Figure 12), exhibit several along-chain volume fluctuations which have a characteristic wavelength of ~ 80 km; this translates to a time period of ~ 0.8–1.1 Myr, depending on the speed of the plate over the source.

Non-point-source models of seamount volcanism could explain these along-chain volume variations by appealing to a mantle source which varies in space or time. For point-source models, such as miniplumes or discrete mantle heterogeneities (Figure 17a), the seamount source variation must be temporal, requiring pulses of material from a miniplume or changes in the size of an upwelling heterogeneity along a mantle stream-line.

Relationships between adjacent chains

The extent to which seamount chains are interrelated, beyond simply their association in the abundant Rano Rahi Field, may provide insight into models of their formation. Do nearby seamount chains share the same source, or do they have distinct sources which somehow influence each other?

The seamount chains of the Pacific Plate have a consistent minimum spacing of 15–20 km between their axes. It is likely that some adjacent chains were active simultaneously, especially the relatively long chains on young crust. Shen *et al.* (1995) perform statistical analyses which show that the along-chain variations in seamount volume of adjacent seafloor corridors are correlated with each other; they are not independent and random. These volume trade-offs are most easily seen between the Hurihuri and eastern Cloud chains (Figure 12) and among the Anakena, Toroko, and Chapple chains (Shen *et al.*, 1993). Shen *et al.* (1995) conclude that the zone of influence of the source of a given chain may extend to adjacent chains. If this proves to be the case in general, it is difficult to envision how a distribution of embedded heterogeneities could bring about this covariance. Given a miniplume model, the pulsing of flux from a given plume would necessarily be related to that of other plumes 15–20 km away.

The spacing of seamount chains may be a function of lithospheric plate strength. When a seamount loads a plate having some strength, the resulting deflection produces stresses in the plate which may aid or hinder the passage of magma (ten Brink, 1991). The lateral extent of flexural depressions surrounding large seamounts in this area is ~ 10 km (Scheirer *et al.*, in prep.), approximately half of the minimum chain spacing. If the spacing of chains is governed by properties of the overlying plate, then the abundance of chains at this minimum spacing might signify the widespread availability of melt beneath the lithosphere. The spacing of volcanoes along individual seamount chains, however, can be as small as 1–2 km. Thus, if there are properties of the plate which prohibit seamount chains from forming too close together, then another process governs the edifice spacing along an individual chain.

Minor, yet significant, differences in chain orientation exist among adjacent chains, most obvious with the Anakena, Toroko, and Chapple chains. The spacing, measured parallel to the spreading axis, between Anakena and Toroko nearly doubles from 16 to 28 km approaching the axis from 100 km to 25 km. This suggests that, while some seamount sources may influence each other, they are distinct enough to migrate with respect to one another.

Seamounts related to gravity lineaments

The gravity lineaments of Haxby and Weissel (1986) were observed in Seasat altimetry to extend from ~ 6 Ma on the Pacific Plate out to the hot spot islands of the south-central Pacific. These free-air gravity anomalies are 10–20 mgal in amplitude, range in wavelength from 150–250 km, and parallel the current absolute and relative plate motion directions. Recent shipboard gravity and bathymetry analysis (Scheirer *et al.*, in prep.) shows that at least two of the lineaments continue towards the SEPR, in more muted form, to crust aged less than 2 Ma. The shipboard anomalies have similar wavelengths to the altimetry-defined lineaments but are nearly east-west in orientation. Given the disparate spacings of the gravity lineaments and of seamount chains, most individual chains cannot be simply associated with individual gravity lineaments (Figure 18). The north-south extent of the main part of the Rano Rahi Field, from 17°–19° S, corresponds to the projection of two gravity lineament negative anomalies and the intervening positive.

Two striking examples of a correspondence between seamounts and gravity lineaments occur for the far off-axis and extensively active seamount chains in the western corners of the survey, Hotu Matua (Figure 4e) and Apitoka. These chains fall within gravity lineament lows both in shipboard measurements and in the altimetry. The Hotu Matua cluster of seamounts are aligned east-west, along the trend of the lineaments seen nearer the axis, while the Apitoka Ridge is closer in orientation to the plate motion trends, parallel to the gravity lineaments beyond ~ 6 Ma. Sandwell *et al.* (submitted) describe the Pukapuka Ridge System which extends over 2500 km from the western edge of our survey to the Tuamotu Archipelago and is also restricted to a gravity trough. Not all of the gravity lineament negatives in the western part of the survey are associated with seamount chains; the negative anomaly centered at 16° 10′ S, has only a few sea-

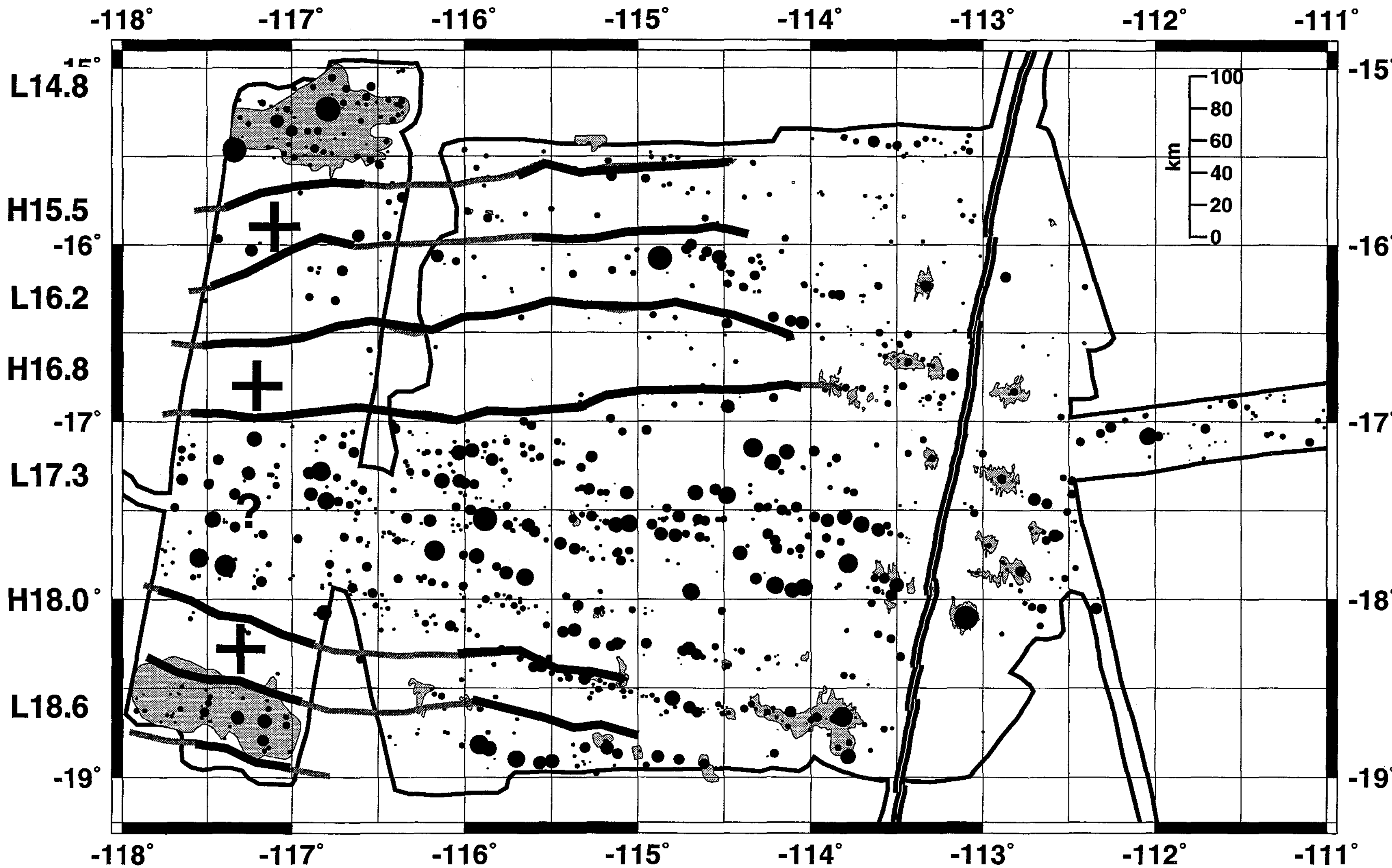

Fig. 18. SEPR seamounts and outlines of the intermediate wavelength gravity lineaments identified by Scheirer *et al.* (in prep.) from shipboard gravity anomalies. Plus symbols indicate positive anomalies, and gray lines indicate suspected lineament boundaries, and gray-shaded areas correspond to reflective seafloor.

mounts. However, the adjacent regions of positive anomalies are virtually devoid of seamounts.

To test the notion that there are more and larger seamounts in the troughs of gravity lineaments than along gravity highs, we count and calculate the volume of seamounts which lie on seafloor identified as unambiguously belonging to negative or positive lineament anomalies from the shipboard gravity, Figure 19. Although the complicating gravitational effects of the abundant seamount chains hinder gravity lineament identification near the center of the Rano Rahi Field, elsewhere there are clear increases in the number and especially the volume of seamounts associated with intermediate-wavelength, negative gravity anomalies.

The causal connection between the formation of the gravity lineaments and some of the seamounts is currently unclear. If the lineaments were caused by on-going ridge-perpendicular convection, then upwelling zones would correspond to shallow seafloor and the corresponding positive free-air anomalies would be the most likely locations for seamount magmas to form in the mantle, Figure 17b. However, the observed active volcanism occurs in zones of deep seafloor. Alternatively, if the lineaments were formed by stretching of the lithosphere (Figure 17c), then the seamounts would most likely form in areas of deep seafloor (as is observed) and thinned plate (Sandwell *et al.*, submitted).

Seamounts related to asymmetric subsidence

From the Yaquina Transform (~ 6° S) to the Easter Microplate (23°S), Pacific Plate younger than 12 Ma subsides at an anomalously low rate, <225 m/Myr$^{1/2}$ (Cochran, 1986); this is significantly slower than the Nazca flank (375 m/Myr$^{1/2}$) and the average global subsidence rates (350 m/Myr$^{1/2}$). The subsidence asymmetry could be explained by a change in the physical properties of the mantle about the axis and/or by a change in the thermal structure of the asthenosphere. In the latter scenario, to fit the low Pacific subsidence, Cochran (1986) modeled an average temperature increase in the asthenosphere of 0.1°/km above a compensation depth of 150 km, from the SEPR out to plate aged ~ 12 Ma. This would result in the asthenosphere beneath the westernmost part of the survey area being ~ 100° hotter than that beneath the axis. Such a thermal gradient (increasing asthenospheric temperature away from the axis) is unusual, but might, in some way, be related to the anomalous Superswell region >2500 km to the west (McNutt and Fischer, 1987; McNutt and Judge, 1990). Alternatively, ridge-perpendicular convection might deliver heat to the base of the lithosphere in the west flank to slow the subsidence of Pacific seafloor (Buck and Parmentier, 1986; Parsons and McKenzie, 1978).

The seafloor in this study area subsides at virtually the same rate in both the seamount-poor northern half and in the seamount-rich southern half; thus, a local correspondence between low Pacific subsidence rates and seamount abundance is not present. More extensive coverage of the Nazca flank, however, is needed to determine if seamount abundance reflects the asymmetry in subsidence rate.

Active seamounts and their proximity to the SEPR

The observation that fresh lava flows are associated with seamounts both near to (<20 km) and far from (>400 km) the axis favors multiple processes for the creation of the Rano Rahi Seamounts. The model of early melting of embedded, fertile heterogeneities in the upwelling zone beneath the spreading center (Figure 17a) predicts that active volcanism will occur within ~ 20 km (for narrow upwelling models) or within ~ 100 km (for wide upwelling models) of the ridge axis. If secondary, e.g. ridge perpendicular, upwelling caused the melting of embedded heterogeneities (Figure 17b), then this convection would necessarily extend deeper in the mantle than the zone already depleted by melting at the ridge axis, since any shallower heterogeneity would have been tapped during upwelling beneath the axis.

Some of the proposed models of seamount formation have difficulties producing seamounts very near the axis; existing models of ridge-perpendicular convection (Figure 17b) and north-south extension (Figure 17c) both require a significant off-axis distance to form (more than a few million years, according to the parameters of Buck and Parmentier (1986) and Dunbar and Sandwell (1988)). Varying the model parameters, e.g. by assuming lower asthenosphere viscosities, would allow ridge-perpendicular convection to occur closer to the axis.

Seamount abundance and superfast spreading rates

Considering a global dataset, Scheirer and Macdonald (1995) observe a more or less linear increase in the abundance of near-axis seamounts with spreading rate. Overall, the SEPR seamounts are consistent with this relationship at the superfast spreading end. Whatever mechanism or mechanisms are important for seamount formation seem to be most effective at produ-

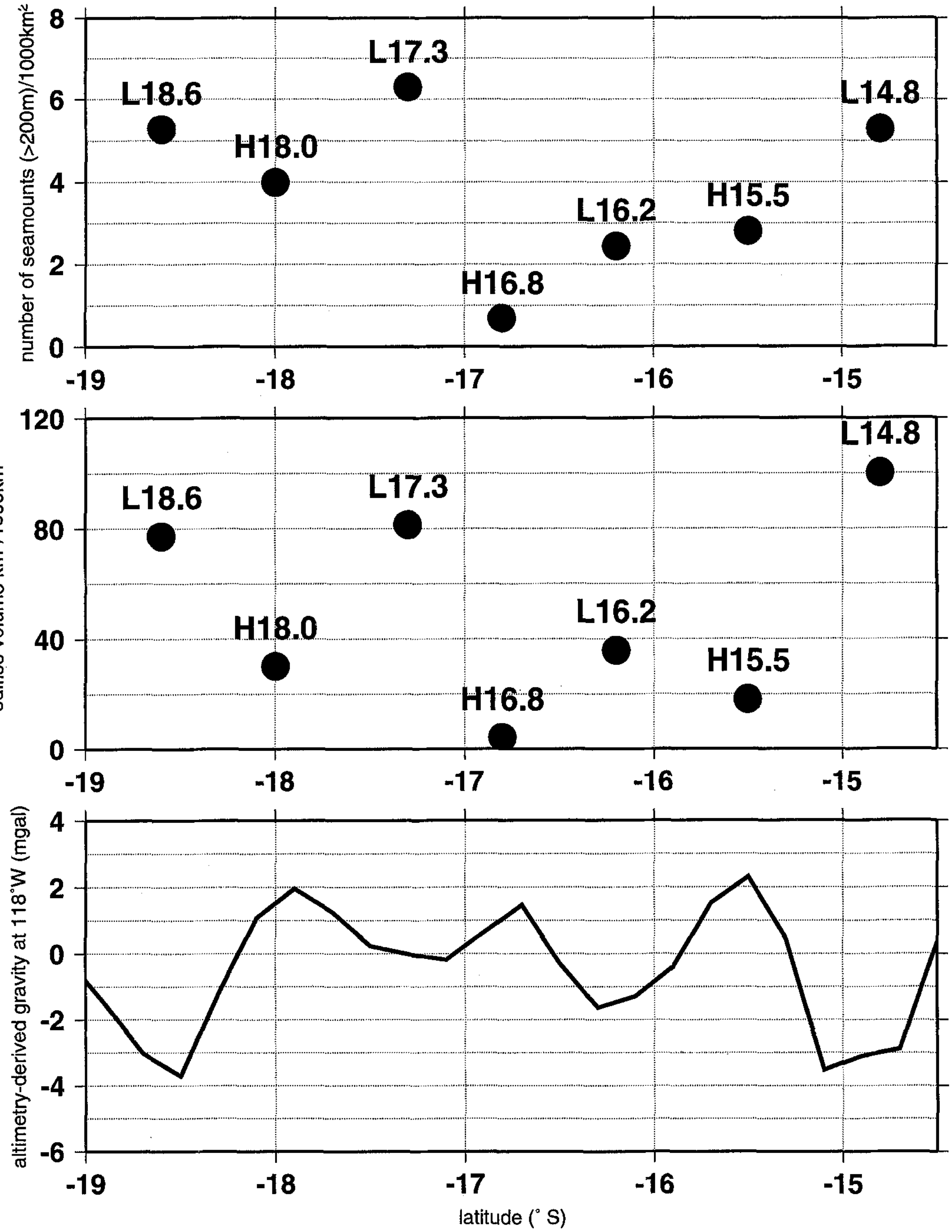

Fig. 19. The abundance (top) and volume (middle) of seamounts, normalized to bathymetry coverage, which fall within well-defined gravity lineaments based on shipboard gravity. Lineaments are named as gravity highs (H) or lows (L) followed by the latitude at which they intersect 118° W. (bottom) The altimetry-defined gravity anomaly along 118° W, calculated by east-west projecting Seasat, Geosat, and ERS1-derived gravity anomalies falling within ±100 km of 118° W.

cing seamounts near superfast spreading centers; perhaps this is because the lithosphere thickens at greater distances from the axis and because mantle upwelling and crustal production rates are the greatest of any spreading center away from a hot spot (Scheirer and Macdonald, 1995). However, the change in spreading rate is negligible from the northern half to the southern half of the 15°–19° S area, so these processes cannot explain finer-scale variation in observed seamount abundance. The lack of coverage on the east flank hinders evaluation of whether the abundance of seamounts on the Pacific Plate is most likely simply a function of the superfast spreading or to some special conditions beneath the Pacific seafloor.

Assessing the Proposed Models of Seamount Formation

As discussed above, the variety in seamount morphology, activity, and setting implies that more than one mechanism is at work to produce the Rano Rahi seamounts. Seamounts are active both very near to and far from the SEPR; some seamount chains are most likely associated with point-sources while others seem to have more two-dimensional sources. The following assessments of the proposed models may be made from our observations:

1. *Embedded fertile heterogeneity source (Figure 17a)*: This model may apply to the seamounts active near the axis, especially to those which seem to have a point source and are active only towards their near-axis ends. The heterogeneities would need to be very elongated or clustered approximately along mantle flow-lines to produce chains 60 km or more in length. Slight departures in the orientation of the heterogeneity from a vertical mantle flow-line could produce different orientations for the seamount chains. For embedded fertile mantle heterogeneties to be the source of the seamount magmas further from the axis (>100 km), then some secondary convection needs to extend to depths deeper than the initial melting depths of MORB beneath the axis. This embedded heterogeneity model would have difficulties in accounting for the wide-spread, voluminous volcanism occurring along the entire lengths of a number of the Pacific chains far from the axis. Although the exact nature and extent of compositional heterogeneities in the asthenosphere is not known, blebs and streaks of heterogeneous material are generally thought to exist in the mantle, and these may be important for off-axis volcanism (Gurnis, 1986; Kellogg and Turcotte, 1990; Sleep, 1984; Wilson, 1992; Zindler *et al.*, 1984).
2. *Miniplumes (Figure 17a)*: This model differs from the above one primarily by its implication that a mantle anomaly (thermal or compositional) can generate melt independently of other mantle upwelling; thus, it might explain the recent activity farther from the axis better than the embedded heterogeneity model. If this model applies to the chains near the axis and if there is a wide zone of upwelling and primary melt production, then some means of keeping the seamount melt volume separate from that which erupts on-axis is needed (e.g. the solitary waves of Richter and Daley (1989)). The nature of the unstable layer feeding the plumes is unknown (Shen *et al.*, 1995), but the influence of adjacent miniplumes on each other may explain the covariation of edifice size among a number of the larger seamount chains.
3. *Mantle upwelling associated with ridge-perpendicular convection (Figure 17b)*: This model could produce off-axis, non-point-source volcanism and may cause the recent lava flows at Hotu Matua and Apitoka, as well as the long Pukapuka Ridge System if ridge-perpendicular convection is the primary cause of the intermediate-wavelength gravity lineaments. A significant difficulty, though, is that this model predicts that the upwelling, melt production, and seamount formation would occur in regions of shallow seafloor; this is counter to observations.
4. *Lithospheric stretching (Figure 17c)*: This proposed mechanism for the formation of the gravity lineaments might also be responsible for the formation of off-axis seamounts. In this model, bathymetric lows would be associated with thinned lithosphere (and possible minor upwelling) where preferential seamount formation would occur; this association of bathymetry lows and abundant seamounts is observed. However, two observations suggest that this stretching, as proposed (Dunbar and Sandwell, 1988; Sandwell and Dunbar, 1988), is not the cause of the lineaments. Locally, there is no evidence for structures on the seafloor associated with north-south extension, even for lineaments away from seamounts. Regionally, fracture zones separated by many gravity lineaments do not show any evidence for increased separation on the Pacific Plate relative to their counterparts on the Nazca Plate (where similar gravity lineaments do not exist), indicating that north-south extension is much smaller than that required to create the gravity lineaments (Goodwillie and Parsons, 1992).
5. *Three-dimensional, time-dependent convection*: This model may run into problems in explaining the long duration of individual chains (often inferred to be active for more than 1 Myr) and the relatively stable geometry of neighboring chains. However, the predictions from this model are not specific enough to test with the available bathymetry and morphological data.
6. *Unusual properties of the Pacific Plate and asthenosphere (Figure 17d)*: In addition to the unusual

features of the Pacific Pate mentioned above (low subsidence, presence of gravity lineaments, abundant seamounts), a recent isotopic study of SEPR lavas suggest that a discrete and broad mantle heterogeneity having a mildly plume-like isotopic signature may be entering the SEPR melt zone in the northern part of the survey area (Mahoney *et al.*, 1994). With their axial dataset, they cannot determine whether the heterogeneity derives from below, from the east, or from the west of the axis, but a broad plume-like zone may underlie the Pacific Plate. The relationships of such an anomaly to the production and distribution of melt away from the axis, its effects on the overlying plate, and to possible return flow from the hotspots of the Superswell, are unknown. The asymmetry in seafloor subsidence may arise from a thermal anomaly in the asthenosphere (Cochran, 1986), hotter to the west, which might be related to the isotopic plume. However, the along-axis extent of the asymmetric subsidence from 9° S to 23° S is much greater than the extents of both the geochemical anomaly (Mahoney *et al.*, 1994) and the Rano Rahi Seamount Field.

Finally, we note that the SEPR's relatively rapid migration (~ 30 mm/yr) to the west-northwest might entrain and melt any fertile mantle heterogeneities preferentially beneath the Pacific Plate, according to the model of Davis and Karsten (1986). This would impart an asymmetry in the abundance of near-axis seamounts about the SEPR, with more seamounts on the Pacific flank. Evaluating such an asymmetry is ambiguous with the available dataset.

The above models of seamount formation concentrate on the mantle source of seamount magmas, assuming in most cases that the lithosphere is largely penetrable by any melt volume at its base. This assumption is clearly an oversimplification, and the decrease of new seamounts with distance from the axis may well be primarily a function of the thickening lithospheric plate. Properties of the plate might ultimately dictate which melt volumes ascend through the lithosphere and which do not. Weakening of the lithosphere might occur at a range of scales, from regional plume-like reheating or stretching, to deformation associated with ridge-perpendicular convection, to flexural effects of large seamount chains.

Another outstanding problem, which is related to models of near-axis seamount formation but which is only moderately addressable with this morphologic dataset, is the growth rates and histories of individual edifices. Most of the discussion, above, assumes that the volcanoes form more or less instantaneously with respect to the rates of other geologic processes (plate-spreading, magnetic field variation). The combined magnetization and seafloor reflectivity analysis indicates that some of the chains may have had a multi-stage growth history, although the volumetric importance of these stages is unknown. Likewise, the possibility that late-stage lavas erupt from the flanks or bases of volcanoes is one which needs to be explored with higher resolution mapping systems. More precise geochronologic and geochemical analysis of rocks sampled from different parts of individual seamounts and across the Rano Rahi Field should elucidate their sources and evolution and allow better comparisons to be made between these seamounts and terrestrial basaltic volcanoes.

Summary

The Rano Rahi Field is distinctive because of its great seamount abundance and the widespread off-axis volcanic activity on a wide range of seafloor ages. Most of the seamounts belong to chains closely aligned to the absolute and relative plate motion directions of the Pacific Plate although several have significant but independent bends. Near the axis, seamount chains are generally composed of distinct, circular edifices. Several hundred kilometers from the axis, the typical seamount chain is composed of edifices which overlap at their bases; still further, ridges comprise the main volcanic construction. Some of the chains split into two, and others seem to build at the expense of nearby chains. Evidence for recent, reflective lava flows suggests that some chains are mainly formed by point-sources whereas others arise from more two-dimensional sources. Widespread, young lava flows surrounding some seamounts and volcanic ridges exhibit reversed magnetization, suggesting at least a two-stage growth history with an early edifice-forming stage prior to ~ 0.8 Ma followed by an areally extensive lava flow < 0.2 Ma.

Relative to the NEPR seamounts, those near the SEPR are about three times as abundant and appear to be active over a much wider age range (> 6 Myr vs. < 1 Myr). The SEPR seamount chains are generally longer, more closely spaced, and align better with the plate motion directions than their counterparts near the NEPR. Different models for seamount formation seem to apply for seamounts in different areas. Point-source models such as embedded heterogeneities and miniplumes may best apply to seamounts within ~ 70 km of the axis. Further from the axis, the cause of the extensive gravity lineaments might also produce the seamounts on older plate, whether by convection or some manner of extension in the Pacific lithosphere. We emphasize that, at present, the relationships between melting at depth and its manifestation as seafloor volcanism are poorly understood. More detailed study of seamount morphology and geochemistry will yield greater insight into these processes than available with this sea surface-derived dataset.

Acknowledgements

We thank Doug Wilson and Tanya Atwater for reviews of this manuscript in an early form. Two anonymous reviews also improved the submitted manuscript substantially. Deborah Smith provided the code to perform the maximum likelihood regression. This research was supported by NSF OCE89-11587.

Appendix

The table containing all of the Rano Rahi seamount measurements is available as a tab-delimited ASCII file: sepr__seamount__table, via anonymous ftp from rapa.geol.ucsb.edu (128.111.108.25), in directory /pub/MGR.sepr__grids. This directory also contains the bathymetry grids used in the companion map series paper. The file: README.sepr__seamount__table contains documentation about the seamount table.

References

Abers, G. A., Parsons, B., and Weissel, J. K., 1988, Seamount abundances and distributions in the southeast Pacific, *Earth Planet. Sci. Lett.* **87**, 137–151.

Barone, A. and Ryan, W. B. F., 1990, Single plume model for asynchronous formation of the Lamont seamounts and adjacent East Pacific Rise terrain, *J. Geophys. Res.* **95**, 10801–10827.

Barr, S. M., 1974, Seamount chains formed near the crest of Juan de Fuca Ridge, northeast Pacific Ocean, *Mar. Geol.* **17**, 1–19.

Bemis, K. G. and Smith, D. K., 1993, Production of small volcanoes in the Superswell region of the South Pacific, *Earth Planet. Sci. Lett.* **118**, 251–263.

Buck, W. R. and Parmentier, E. M., 1986, Convection beneath young oceanic lithosphere: Implications for thermal structure and gravity, *J. Geophys. Res.* **91**, 1961–1974.

Clague, D. A. and Dalrymple, G. B., 1989, Tectonics, geochemistry, and origin of the Hawaiian-Emperor volcanic chain, in *The Geology of North America,* Winterer, E. L., Hussong, D. M., and Decker, R. W. (eds.), Geological Society of America, Boulder, Colorado, pp. 188–217.

Cochran, J. R., 1986, Variation in subsidence rates along intermediate and fast spreading mid-ocean ridges, *Geophys. J. R. Astron. Soc.* **87**, 421–454.

Cormier, M.-H. and Macdonald, K. C., 1994, East Pacific Rise 18°–19°S: Asymmetric spreading and ridge reorientation by ultrafast migration of axial discontinuities, *J. Geophys. Res.* **99**, 543–564.

Cormier, M.-H., Scheirer, D. S., and Macdonald, K. C., 1996, Evolution of the East Pacific Rise at 16°–19° S since 5 Ma: Bisection of Overlapping Spreading Centers by New, Rapidly Propagating Ridge Segments, *Mar. Geophys. Res.* **18**, 53–84 (this issue).

Davis, E. E. and Karsten, J. L., 1986, On the cause of the asymmetric distribution of seamounts about the Juan de Fuca Ridge: Ridge-crest migration over a heterogeneous asthenosphere, *Earth Planet. Sci. Lett.* **79**, 385–396.

Dekov, V. M. and Kupstov, V. M., 1990, Rates of accumulation of metal-bearing sediments on the East Pacific Rise (20° S), *Oceanology* **30**, 321–324.

Dekov, V. M. and Kuptsov, V. M., 1992, Late Quaternary rates of accumulation of metal-bearing sediments on the East Pacific Rise, *Oceanology* **32**, 94–101.

DeMets, C., Gordon, R. G., Argus, D. F., and Stein, S., 1990, Current plate motions, *Geophys. J. Int.* **101**, 425–478.

Desonie, D. L. and Duncan, R. A., 1990, The Cobb-Eikelberg seamount chain: Hotspot volcanism with mid-ocean ridge basalt affinity, *J. Geophys. Res.* **95**, 12697–12711.

Detrick, R. S., Buhl, P., Vera, E., Mutter, J., Orcutt, J., Madsen, J., and Brocher, T., 1987, Multi-channel seismic imaging of a crustal magma chamber along the East Pacific Rise, *Nature* **326**, 35–41.

Detrick, R. S., Harding, A. J., Kent, G. M., Orcutt, J. A., Mutter, J. C., and Buhl, P., 1993, Seismic structure of the southern East Pacific Rise, *Science* **259**, 499–503.

Dunbar, J. and Sandwell, D. T., 1988, A boudinage model for crossgrain lineations, *EOS Trans. AGU* **69**, 1429.

Edwards, M. H., Fornari, D. J., Malinverno, A., Ryan, W. B. F., and Madsen, J., 1991, The regional tectonic fabric of the East Pacific Rise from 12° 50' N to 15° 10' N, *J. Geophys. Res.* **96**, 7995–8017.

Goodwillie, A. M. and Parsons, B., 1992, Placing bounds on lithospheric deformation in the central Pacific Ocean, *Earth Planet. Sci.* **111**, 123–139.

Gripp, A. E. and Gordon, R. G., 1990, Current plate velocities relative to the hotspots incorporating the NUVEL-1 plate motion model, *Geophys. Res. Lett.* **17**, 1109–1112.

Gurnis, M., 1986, Stirring and mixing in the mantle by plate-tectonic flow: Large persistent blobs and long tendrils coexist, *Geophys. Res. Lett.* **13**, 1464–1467.

Haxby, W. F. and Weissel, J. K., 1986, Evidence for small-scale convection from Seasat altimeter data, *J. Geophys. Res.* **91**, 3507–3520.

Jordan, T. H., Menard, H. W., and Smith, D. K., 1983, Density and size distribution of seamounts in the eastern Pacific inferred from wide-beam sounding data, *J. Geophys. Res.* **88**, 10508–10518.

Kellogg, L. H. and Turcotte, D. L., 1990, Mixing and the distribution of heterogeneities in a chaotically convecting mantle, *J. Geophys. Res.* **95**, 421–432.

Kleinrock, M. C., Brooks, B. A., and Smith, D. K., 1994, Construction and destruction of volcanic knobs at the Cocos-Nazca spreading system near 95° W, *Geophys. Res. Lett.* **21**, 2307–2310.

Lonsdale, P., 1989, Segmentation of the Pacific-Nazca spreading center, 1° N–20° S, *J. Geophys. Res.* **94**, 12197–12226.

Lyle, M., Leinen, M., Owen, R. M., and Rea, D. K., 1987, Late Tertiary history of hydrothermal deposition at the East Pacific Rise, 19° S: correlation to volcano-tectonic events, *Geophys. Res. Lett.* **14**, 595–598.

Macdonald, K. C., Fox, P. J., Miller, S., Carbotte, S., Edwards, M. H., Eisen, M., Fornari, D. J., Perram, L., Pockalny, R., Scheirer, D., Tighe, S., Weiland, C., and Wilson, D., 1992, The East Pacific Rise and its flanks 8°–18° N: History of segmentation, propagation and spreading direction based on SeaMARCII and Sea Beam studies, *Mar. Geophys. Res.* **14**, 299–344.

Mahoney, J. J., Sinton, J. M., Kurz, M. D., Macdougall, J. D., Spencer, K. J., and Lugmair, G. W., 1994, Isotope and trace element characteristics of a superfast spreading ridge: East Pacific Rise, 13°–23° S, *Earth Planet. Sci. Lett.* **121**, 173–193.

Mammerickx, J., Anderson, R. N., Menard, H. W., and Smith, S. M., 1975, Morphology and tectonic evolution of the east central Pacific, *Geol. Soc. Am. Bull.* **86**, 111–118.

Marchig, V., Erzinger, J., and Heinze, P. M., 1986, Sediments in the black smoker area of the East Pacific Rise (18.5° S), *Earth Planet. Sci. Lett.* **79**, 93–106.

McNutt, M. K. and Fischer, K. M., 1987, The South Pacific superswell, in *Seamounts, Islands, and Atolls,* Keating, B. H., Fryer, P., Batiza, R., and Boehlerg, G. W. (eds.), Geophysical Monograph 43, American Geophysical Union, Washington, D.C., pp. 25–34.

McNutt, M. K. and Judge, A. V., 1990, The superswell and mantle dynamics beneath the South Pacific, *Science* **248**, 969–975.

Menard, H. W.: 1964, [Marine Geology of the Pacific], McGraw Hill, New York.

Moore, J. G., Normark, W. R., and Holcomb, R. T., 1994, Giant Hawaiian Landslides, *Ann. Rev. Earth Planet. Sci.* **22**, 119–144.

Naar, D. F. and Hey, R. N., 1989, Recent Pacific-Easter-Nazca plate motions, in *Evolution of Mid-Ocean Ridges,* Sinton, J. M. (ed.), IUGG Geophysical Monograph 57, pp. 9–30.

Parsons, B. and McKenzie, D., 1978, Mantle convection and the thermal structure of plates, *J. Geophys. Res.* **83**, 4485–4496.

Perram, L. J., Cormier, M. -H., and Macdonald, K. C., 1993, Magnetic and tectonic studies of the duelling propagating spreading centers at 20° 40' S on the East Pacific Rise: Evidence for crustal rotations, *J. Geophys. Res.* **98**, 13835–13850.

Renard, V., Hekinian, R., Francheteau, J., Ballard, R. D., and Bäcker, H., 1985, Submersible observations at the axis of the ultra-fast spreading East Pacific Rise (17° 30' S to 21° 30' S), *Earth Planet. Sci. Lett.* **75**, 339–353.

Richter, F. M. and Daley, S. F., 1989, Dynamical and chemical effects of melting a heterogeneous source, *J. Geophys. Res.* **94**, 12499–12510.

Sandwell, D. T. and Dunbar, J., 1988, Stretching of the central Pacific lithosphere: Super swell, crossgrain lineations and en-echelon ridges, *EOS Trans. AGU* **69**, 1429.

Sandwell, D. T., Winterer, E. L., Mammerickx, J., Duncan, R. A., Lynch, M. A., Levitt, D., and Johnson, C. L., submitted, Evidence from the Pukapuka Ridges for diffuse extension of the Pacific Plate: No mini hotspots, no convection, *J. Geophys. Res.*

Scheirer, D. S., Forsyth, D. W., and Macdonald, K. C., in prep., The development of lineaments in the gravity field near the Southern East Pacific Rise.

Scheirer, D. S. and Macdonald, K. C., 1993, Variation in cross-sectional area of the axial ridge along the East Pacific Rise: Evidence for the magmatic budget of a fast spreading center, *J. Geophys. Res.* **98**, 7871–7885.

Scheirer, D. S. and Macdonald, K. C., 1995, Near-axis seamounts on the flanks of the East Pacific Rise, 8° N to 17° N, *J. Geophys. Res.* **100**, 2239–2259.

Scheirer, D. S., Macdonald, K. C., Forsyth, D. W., and the Gloria Legs 2 and 3 Scientific Parties, 1993, An extensive seamount field near the Southern East Pacific Rise 15° to 19° S, *Eos Trans. AGU, Spring Meeting suppl.* **73**, (16), 297.

Scheirer, D. S., Macdonald, K. C., Forsyth, D. W., Miller, S. P., Wright, D. J., Cormier, M. -H., and Weiland, C. M., this issue, A map series of the southern East Pacific Rise and its flanks, 15°–19° S, *Mar. Geophys. Res.*

Scheirer, D. S., Macdonald, K. C., Forsyth, D. W., and the Gloria 2 and 3 Scientific Parties, 1993, Wide-spread volcanic and tectonic activity on the Southern East Pacific Rise and its flanks, *Ridge Newsletter* **4**, 1–2, 8–10.

Shen, Y., Forsyth, D. W., Scheirer, D. S., and Macdonald, K. C., 1993, Two forms of volcanism: implications for mantle flow and off-axis crustal production on the west flank of the southern East Pacific Rise, *J. Geophys. Res.* **98**, 17875–17889.

Shen, Y., Scheirer, D. S., Forsyth, D. W., and Macdonald, K. C., 1995, Trade-off in production of adjacent seamount chains near the East Pacific Rise, *Nature* **373**, 140–143.

Sinton, J. M., Hall, L. S., and Batiza, R., 1993, Geochemistry of the Rano Rahi Seamounts: mantle melting within 450 km of the East Pacific Rise, 15.5–19° S, *EOS Trans. AGU* **74**, Fall Meeting Supplement, 687.

Sinton, J. M., Smaglik, S. M., Mahoney, J. J., and Macdonald, K. C., 1991, Magmatic processes at superfast spreading mid-ocean ridges: glass compositional variation along the East Pacific Rise 13°–23° S, *J. Geophys. Res.* **96**, 6133–6155.

Sleep, N. H., 1984, Tapping of magmas from ubiquitous mantle heterogeneities: an alternative to mantle plumes?, *J. Geophys. Res.* **89**, 10029–10041.

Smith, D. K., 1988, Shape analysis of Pacific seamounts, *Earth Planet. Sci. Lett.* **90**, 457–466.

Smith, D. K. and Cann, J. R., 1992, The role of seamount volcanism in crustal construction at the Mid-Atlantic Ridge (24°–30° N), *J. Geophys. Res.* **97**, 1645–1658.

Smith, D. K. and Jordan, T. H., 1987, The size distribution of Pacific seamounts, *Geophys. Res. Lett.* **14**, 1119–1122.

ten Brink, U., 1991, Volcano spacing and plate rigidity, *Geology* **19**, 397–400.

Trial, A. F. and Spera, F. J., 1990, Mechanisms for the generation of compositional heterogeneities in magma chambers, *G.S.A. Bull.* **102**, 353–367.

Wilson, D. S., 1992, Focused mantle upwelling beneath mid-ocean ridges: Evidence from seamount formation and isostatic compensation of topography, *Earth Planet. Sci. Lett.* **113**, 41–55.

Winterer, E. L. and Sandwell, D. T., 1987, Evidence from en-echelon crossgrain ridges for tensional cracks in the Pacific plate, *Nature* **329**, 534–537.

Zindler, A., Staudigel, H., and Batiza, R., 1984, Isotopic and trace element geochemistry of young Pacific seamounts: implications for the scale of upper mantle heterogeneity, *Earth Planet. Sci. Lett.* **70**, 175-195.